Simulations reveal insidious challenges to artificial community selection and possible strategies for success

Li Xie* , Alex E. Yuan, and Wenying Shou*

Basic Sciences Division, Fred Hutchinson Cancer Research Center, Seattle, WA, 98109

Abstract

Multi-species microbial communities often display "community functions" stemming from interactions of member species. Interactions are often difficult to decipher, making it challenging to design communities with desired functions. Alternatively, similar to artificial selection for individuals in agriculture and industry, one could repeatedly choose communities with the highest community functions to reproduce by randomly partitioning each into multiple "Newborn" communities for the next cycle. However, previous efforts in selecting complex communities have generated mixed outcomes that are difficult to interpret. To understand how to effectively enact community selection, we simulated community selection to improve a community function that requires two species and imposes a fitness cost on one or both species. Our simulations predict that improvement could be easily stalled unless various aspects of selection, including species choice, selection regimen parameters, and stochastic populating of Newborn communities, were carefully considered. When these considerations were addressed in experimentally feasible manners, community selection could overcome natural selection to improve community function, and in some cases, even force species to evolve to coexist. Our conclusions hold under various alternative model assumptions, and are thus applicable to a variety of communities.

Introduction

Multi-species microbial communities often display important *functions*, defined as biochemical activities not achievable by member species in isolation. For example, a six-species microbial community, but not any member species alone, cleared relapsing *Clostridium difficile* infections in mice [1]. Community functions arise from *interactions* where an individual alters the physiology of another individual. Thus, to improve community function, one could identify and modify interactions [2, 3]. In reality, this is no trivial task: each species can release tens or more compounds, many of which may influence the partner species in diverse fashions [4, 5, 6, 7]. From this myriad of interactions, one would then need to identify those critical for community function, and modify them by altering species genotypes or the abiotic environment. One could also artificially assemble different combinations of species or genotypes at various ratios to screen for high community function. However, the number of combinations becomes

*Authors of correspondence

very large even for a moderate number of species and genotypes, and some species may not be culturable in isolation.

In an alternative approach, artificial selection of whole communities could be carried out over cycles to improve community function [8, 9, 10, 11, 12] (reviewed in [13, 14, 15]). A selection cycle starts with a collection of low-density communities with artificially-imposed boundaries (e.g. inside culture tubes). These low-density communities are incubated for a period of time during which community members multiply and interact with each other and possibly mutate, and the community function of interest develops. At the end of incubation, desired communities are chosen to "reproduce" where each is randomly partitioned into multiple low-density communities to start the next cycle. Superficially, this process may seem straightforward since "one gets what one selects for". After all, artificial selection on individuals has been successfully implemented to obtain, for example, proteins of enhanced activities (Figure S1). However, compared to artificial selection of individuals or mono-species groups, artificial selection of multi-species communities is more challenging. One reason is that community function has limited heredity, since species and genotype compositions can change rapidly from one selection cycle to the next due to ecological and evolutionary forces (see detailed explanation in Figure S1). For example, member species critical for community function may get lost during growth and selection cycles.

The few attempts of community selection have generated interesting results. One theoretical study simulated artificial selection on multi-species communities based on their ability to modify their abiotic environment [10]. Communities responded to selection, but the response quickly leveled off, and could be generated without mutations. Thus, in this case, selection acted on species types instead of new genotypes [10]. In experiments, complex microbial communities were selected to improve their abilities to degrade a pollutant or to alter plant physiology [8, 9, 12, 11]. For example, microbial communities selected to promote early or late flowering in plants were dominated by distinct species types [11]. However in other cases, a community trait may fail to improve despite selection, and may improve even without selection [8, 9].

Because communities used in these selection attempts were complex, much remains unknown. First, was the trait under selection a community function or achievable by a single species? If the latter, then community selection may not even be needed. Second, did selection act solely on species types or also on newly-arising genotypes? If the former ([10, 11]), then without immigration of new species, community function may quickly level off [10]. If the latter, then community function could continue to improve as new genotypes evolve. Finally, why might a community trait sometimes fail to improve despite selection [8, 9]?

In this study, we simulated artificial selection on communities with defined species. Our goal is to improve a "costly" community function via selecting for genotypes that promote community function. A community function is costly if any community member's fitness is reduced by contributing to that community function. Costly community functions are common when microbes are engineered to make a product [16]. Community function can also be costly if high community function requires some species to restrain their growth to not out-compete other species. To improve a costly community function, artificial community selection must overcome natural selection which favors low community function.

To understand how to effectively enact community selection to improve a costly community function, we simulated artificial selection of communities consisting of two defined species whose phenotypes can be modified by random mutations. A simplified two-species community would allow us to mechanistically investigate how community members evolved under community selection. Simulations allow us to compare the efficacy of different selection regimens with relative ease. We also designed our simulations to mimic real lab experiments so that our conclusions could guide future experiments. For example, our simulations incorporated not only chemical mechanisms of species interactions (as advocated by [17, 18]), but also experimental procedures (e.g. pipetting cultures during community reproduction).

Model parameters, including species phenotypes, mutation rate, and distribution of mutation effects, were based on a wide variety of published experiments. Note that most previous models focused on binary phenotypes (e.g. contributing or not contributing to community function) [19], and therefore could not model community function improvement if all members started as contributors. We show that artificial community selection can improve a costly community function, but only after circumventing a multitude of failure traps.

Results

We will first introduce the subject of our community selection simulation: a commensal two-species community that converts substrates to a valued product. We will define community function and show that inappropriate definitions lead to selection failures. We will then describe how we simulate artificial community selection. From simulation results, we will demonstrate critical measures that make community selection effective, including promoting species coexistence, suppressing non-contributors, and being mindful about how routine experimental procedures can impede selection. Finally, we show that our conclusions are robust under alternative model assumptions, applicable to mutualistic communities and communities whose member species normally do not coexist. To avoid confusion, we will use "community selection" or "selection" to describe the entire process of artificial community selection (community formation, growth, selection, and reproduction), and use "choose" to refer to the selection step.

A Helper-Manufacturer community that converts substrates into a product

Motivated by previous successes in engineering two-species microbial communities that convert substrates into useful products [20, 21, 22], we numerically simulated selection of such communities. In our community , Manufacturer M can manufacture Product P of value to us (e.g. a bio-fuel or a drug) at a fitness cost to self, but only if helped by Helper H (Figure 1). Specifically, Helper but not Manufacturer can digest an agricultural waste (e.g. cellulose), and as Helper grows biomass, Helper releases Byproduct B at no fitness cost to itself. Manufacturer requires H's Byproduct (e.g. carbon source) to grow (obligatory commensalism). In addition, Manufacturer invests f_P ($0 \leq f_P \leq 1$) fraction of its potential growth to make Product P while using the rest (1-f_P) for its biomass growth. Both species also require a shared Resource R (e.g. nitrogen). Thus, the two species together, but not any species alone, could convert substrates (Waste and Resource) into Product.

During each community selection cycle (Figure 2), low-density "Newborn" H-M communities were assembled, each supplied with a fixed amount of Resource and excess Waste. These Newborn communities were allowed to grow ("mature") over a fixed time T into high-density "Adult" communities. We define community function as the total amount of Product accumulated as a low-density Newborn community grows into an Adult community over maturation time T, i.e. $P(T)$ (Figure 2, top two rows). In Methods Section 7, we explain problems associated with alternative definitions of community function (e.g. per capita production; Figure S2). Community function $P(T)$ is not costly to Helpers, but reduces M's growth rate by fraction f_P (Figure 1). Therefore, artificial selection is necessary to improve community function, since natural selection always favors non-producing M ($f_P = 0$). Later, we will show that for a community function that is costly to both H and M, our conclusions also hold.

Simulating community selection

We simulated four stages of community selection (Figure 2): forming Newborn communities; Newborn communities maturing into Adult communities; choosing highest-functioning Adult communities, and reproducing the chosen Adult communities by splitting each into multiple Newborn communities of the next cycle. Our simulation was individual-based. That is, it tracked phenotypes and biomass of individual H and M cells in each community as cells grew, divided, mutated, or died. Our simulations also tracked dynamics of chemicals (including Product) in each community, and accounted for actual experimental steps such as pipetting cultures during community reproduction. Below is a brief summary of our simulations, with more details in Methods.

Each simulation (Methods Section 6) started with n_{tot} number of Newborn communities. Each Newborn community always started with a fixed amount of Resource and a total biomass close to a target value BM_{target} (see Methods Section 7 for problems associated with not having a biomass target). Waste was always supplied in excess and thus did not enter our equations. Note that except for the first cycle, the relative abundance of species in a Newborn community inherited that of the parent Adult community.

During community maturation, biomass of individual cells grew. The biomass growth rate of an H cell depended on Resource concentration (Monod Equation; Figure S3A; Eq. 23). As H grew, it consumed Resource and simultaneously released Byproduct (Eqs. 21 and 22). The potential growth rate of an M cell depended on the concentrations of Resource and H's Byproduct ([23]; Figure S3B; see experimental support in Figure S4). M cell's actual biomass growth rate was $(1-f_P)$ fraction of M's potential growth rate (Eq. 24). As M grew, it consumed Resource and Byproduct (Eqs. 21 and 22), and released Product at a rate proportional to f_P and M's potential growth rate (Eqs. 8). Once an H or M cell's biomass grew from 1 to 2, it divided into two cells of equal biomass with identical phenotypes, thus capturing experimental observations of continuous biomass increase (Figure S5) and discrete cell division events [24]. Meanwhile, H and M cells died stochastically at a constant death rate. Although mutations can occur during any stage of the cell cycle, we assigned mutations immediately after cell division, where each phenotype of both cells mutated independently.

Mutable phenotypes included H and M's maximal growth rates and affinities for nutrients ("growth parameters"), and M's f_P (the fraction of potential growth diverted for making Product), since these phenotypes have been observed to rapidly change during evolution ([25, 26, 27, 28]). Mutated phenotypes could range between 0 and their respective evolutionary upper bounds. On average, half of the mutations abolished the function (e.g. zero growth rate, zero affinity, or $f_P = 0$) based on experiments on GFP, viruses, and yeast [29, 30, 31]. Effects of the other 50% mutations were bilateral-exponentially distributed, enhancing or diminishing a phenotype by a few percent, based on our re-analysis of published yeast data sets [32] (Figure S6). We held death rates constant, since death rates were much smaller than growth rates and thus mutations in death rates would be inconsequential. We also held release and consumption coefficients constant. This is because, for example, the amount of Byproduct released per H biomass generated is constrained by biochemical stoichiometry.

At the end of community maturation time T, we obtained community function $P(T)$ (the total amount of Product at time T) for each Adult community. The highest-functioning Adult was randomly partitioned into Newborns of the target total biomass BM_{target}. For example, if the chosen Adult had a total biomass of $60BM_{target}$, then each cell would be assigned a random integer from 1 to 60, and those cells with the same random integer would be allocated to the same Newborn. Experimentally, this is equivalent to volumetric dilution using a pipette. Thus, for each Newborn, the total biomass and species ratio fluctuated around their expected values in a fashion associated with pipetting (Methods Section 9). When the highest-functioning Adult was used up for making Newborns, the next highest-functioning

Adult was chosen and reproduced until n_{tot} Newborns were generated for the next selection cycle.

Overcoming the ecological and evolutionary fragility of species coexistence

In order to improve community function, species need to coexist throughout selection cycles. That is, all species must grow at a similar average growth rate within each cycle. Furthermore, species ratio should not be extreme because otherwise, the low-abundance species could be lost by chance during Newborn formation. Species coexistence at a moderate ratio has been experimentally realized in engineered communities [20, 21, 33, 34].

To achieve species coexistence at a moderate ratio in the H-M community, three considerations need to be made. First, the fraction of growth M diverted for making Product (f_P) must not be too large, or else M would always grow slower than H and thus go extinct (Figure 3 top). Second, upon Newborn formation, H can immediately start to grow on Waste and Resource, while M cannot grow until H's Byproduct has accumulated to a sufficiently high level. Thus, H and M's growth parameters (maximal growth rates in excess nutrients; affinities for nutrients) should ideally allow M to grow faster than H at some point during community maturation. Third, to achieve a moderate steady-state species ratio, metabolite release and consumption need to be balanced. Otherwise, the ratio between metabolite releaser and consumer can be extreme [33].

Based on these considerations and published yeast and *E. coli* measurements, we chose H and M's ancestral growth parameters and their evolutionary upper bounds, as well as release, consumption, and death parameters (Table 1, Methods Section 2). This ensured that throughout selection cycles, different species ratios would converge toward a moderate steady state value during community maturation (Figure 3, bottom). Note that if species were not chosen properly, selection might fail due to insufficient species coexistence (e.g. Figure 7A), although as we will show later, community selection could enforce species coexistence when executed properly (Figure 7).

Choosing selection regimen parameters to avoid known failure modes

After having chosen member species with appropriate phenotypes, we need to consider parameters of selection regimen. These parameters include the total number of communities under selection (n_{tot}), Newborn target total biomass (BM_{target}), the amount of Resource added to each Newborn ($R(0)$), the amount of mutagenesis which controls the rate of phenotype-altering mutations (μ), and maturation time (T). Compared to the well-studied problem of group selection where the unit of selection is a mono-species group [35, 36, 37, 38, 39, 40, 41, 42, 43, 44, 45, 46, 47, 48, 49], community selection is more challenging (Discussions; Figure S1). However, the two types of selections do share common aspects (Discussions; Figure S1). Thus, we can apply group selection theory, together with other practical considerations, to better design selection regimen.

If the total number of communities n_{tot} is very large, then the chosen community will likely display a higher community function than if n_{tot} is small, but the experimental setup is more challenging. We chose a total of 100 communities (n_{tot}=100).

If the mutation rate is very low, then community function cannot rapidly improve. If the mutation rate is very high, then non-producers will be generated at a high rate, and as the fast-growing non-producers take over, community function is likely to collapse. Here, we chose μ, the rate of phenotype-altering

mutations, to be biologically realistic (0.002 per cell per generation per phenotype, which is lower than the highest values observed experimentally; Methods Section 4).

If Newborn total biomass BM_{target} is very large, or if the number of doublings within T is very large, then non-producers will take over in all communities during maturation (Figure S8, compare B-D with A), as predicted by group selection theory. On the other hand, if both BM_{target} and the number of generations within T are very small, then mutations will be rare within each cycle, and many cycles will be required to improve community function. Finally, if BM_{target} is very small, then a member species might get lost by chance during Newborn formation. In our simulations, we chose Newborn's target total biomass $BM_{target} = 100$ biomass (50~100 cells). Unless otherwise stated, we fixed the input Resource $R(0)$ to support a maximal total biomass of 10^4, and chose maturation time T so that total biomass would undergo ~6 doublings (increasing from ~100 to ~7000). Thus, by the end of T, $\leq$70% Resource would be consumed by an average community. This meant that when implemented experimentally, we could avoid complications of Resource depletion and stationary phase, while not wasting too much Resource.

Community selection sometimes improves community function through promoting individual growth

We simulated community selection while allowing H and M's growth parameters (maximal growth rates in excess metabolites; affinities for metabolites) and M's f_P to be modified by mutations. As expected, in control simulations where Adult communities were randomly chosen to reproduce, community function was driven to zero by natural selection as fast-growing non-producing M took over (Figure S9C; average f_P declining to zero in Figure S9B).

When we chose highest-functioning Adult communities to reproduce, community function improved (Figure 4B, compare i and ii). Concurrently, f_P remained nearly unchanged while H and M's growth parameters improved (Figure S10), leading to faster H and M growth rates (Figure 4A). Community function improvement was largely due to improved H and M growth, since disallowing mutations in growth parameters greatly diminished community function improvement (Figure 4B, compare i and iii). Here, improved individual growth promoted community function because of our choices of evolutionary upper bounds: Since H could not evolve to grow so fast to overwhelm M, species ratio was maintained at a moderate level (Figure 3B), and faster H and M growth resulted in more Byproduct, larger M populations, and consequently higher Product level. With different choices of evolutionary upper bounds, increasing growth parameters decreased community function due to H dominance (Figure S7), although we will demonstrate that even in this scenario, properly executed community selection can improve community function while promoting species coexistence (Figure 7).

Community selection may not be effective under conditions reflecting common lab practices

While community function improved, it could have improved significantly more. Specifically, when growth parameters were fixed to their respective upper bounds, as occured during community selection (Figure S10C), maximal community function $P^*(T)$ could be achieved at $f_P^* = 0.41$ (Figure 4C). $P^*(T)$ was much higher than what was achieved during community selection (Figure 4C ii dark grey star).

To investigate why community selection failed to improve community function to maximum $P^*(T)$, we repeated our simulations, except that we fixed H and M's growth parameters to their upper bounds (as

occured during community selection; Figure S10C) and only allowed f_P to mutate. This simplification allowed us to focus on the evolutionary dynamics of f_P, and is justified since we obtained similar conclusions regardless of whether we fixed growth parameters (Figure S13).

Could community selection increase ancestral f_P to f_P^* optimal for community function, despite natural selection favoring lower f_P? Despite thousands of selection cycles, f_P and community function $P(T)$ barely improved, and both were far below their theoretical optima (Figure 5A and B).

Common lab practices can generate sufficiently large non-heritable variations in community function to interfere with selection

Why did community selection fail to improve f_P and community function? One possibility is that community function was not sufficiently heritable from one cycle to the next (Figure S1). We therefore investigated the heredity of community function by examining the heredity of community function determinants.

Community function $P(T)$ was largely determined by phenotypes of cells in the Newborn community. This is because maturation time was sufficiently short (~6 doublings) that new genotypes could not rise to high frequencies to significantly affect community function. Since all phenotypes except for f_P were fixed, community function had three independent determinants: Newborn's total biomass $BM(0)$, Newborn's fraction of M biomass $\phi_M(0)$, and the average f_P over all M cells in Newborn $\overline{f}_P(0)$ (Eq 6-10).

A community function determinant is considered heritable if it is correlated between Newborns of one cycle (Figure 6A, bottom row) and their respective progeny Newborns in the next cycle (Figure 6A, color-matched top row). Among the three determinants, $\overline{f}_P(0)$ was heritable (Figure 6B): if a Newborn community had a high average f_P, so would the mature Adult community and Newborn communities reproduced from it. On the other hand, Newborn total biomass $BM(0)$ was not heritable (Figure 6C). This is because when an Adult community reproduced via pipette dilution, the dilution factor was adjusted so that the total biomass of a progeny Newborn community was on average the target biomass BM_{target}. Newborn's fraction of M biomass $\phi_M(0)$, which fluctuated around that of its parent Adult, was not heritable either (Figure 6D). This is because regardless of the species composition of Newborns, Adults would have similar steady state species composition (Figure 3B), and so would their offspring Newborns.

In successful community selections, variations in community function should be mainly caused by variations in its heritable determinants. However, we found that community function $P(T)$ weakly correlated with its heritable determinant $\overline{f}_P(0)$, but strongly correlated with its non-heritable determinants (Figure 6E-G). For example, the Newborn that would achieve the highest function had a below-median $\overline{f}_P(0)$ (left magenta dot in Figure 6E), but had high total biomass $BM(0)$ and low fraction of M biomass $\phi_M(0)$ (Figure 6F, G). In other words, variation in community function is largely non-heritable, as they are contributed by variations in non-heritable determinants.

The reason for strong correlations between $P(T)$ and the two non-heritable determinants became clear by examining community dynamics. Recall that we had chosen maturation time so that Resource was in excess to avoid stationary phase. Thus, a "lucky" Newborn community starting with a higher-than-average total biomass would convert more Resource to Product (dotted lines in top panels of Figure S14). Similarly, if a Newborn started with higher-than-average fraction of H biomass, then H would produce higher-than-average Byproduct which meant that M would endure a shorter growth lag and make more Product (dotted lines in bottom panels of Figure S14).

To summarize, when community function significantly correlated with its non-heritable determinants

(Figure 6F & G), community selection failed to improve community function (Figure 5B).

Reducing non-heritable variations in an experimentally feasible manner promotes artificial community selection

Reducing non-heritable variations in community function should enable community selection to work. One possibility would be to reduce the stochastic fluctuations in non-heritable determinants $BM(0)$ and $\phi_M(0)$. Indeed, when each Newborn received a fixed biomass of H and M (Methods, Section 6), $P(T)$ became strongly correlated with $\overline{f}_P(0)$ (Figure 5L). In this case, both $\overline{f}_P$ and community function $P(T)$ improved under selection (Figure 5, J and K) to near the optimal. $P(T)$ improvement was not seen if either Newborn total biomass or species fraction was allowed to fluctuate stochastically (Figure 5, D-I). $P(T)$ also improved if fixed numbers of H and M cells (instead of biomass) were allocated into each Newborn (Figure S15, A and B; Methods, Section 6). Allocating a fixed biomass or number of cells from each species to Newborn communities could be experimentally realized by using a cell sorter if species have different fluorescence ([50]).

Non-heritable variations in $P(T)$ could also be curtailed by reducing the dependence of $P(T)$ on non-heritable determinants. For example, we could extend the maturation time T to nearly deplete Resource. In this selection regimen, Newborns would still experience stochastic fluctuations in Newborn total biomass $BM(0)$ and fraction of M biomass $\phi_M(0)$. However, all communities would end up with similar $P(T)$ since "unlucky" communities would have time to "catch up" as "lucky" communities wait in stationary phase. Indeed, with this extended T, community function became strongly correlated with $\overline{f}_P(0)$ and community function improved without having to fix Newborn total biomass or species composition (Figure 5, M-O; Figure S15, C and D). However in practice, non-heritable variations in community function could still arise from stochastic fluctuations in the duration of stationary phase (which could affect cell survival or the length of recovery time in the next selection cycle).

As expected, the effectiveness of community selection also depends on the uncertainty in community function measurements - another source of non-heritable variations. When we added to each $P(T)$ a measurement noise (normally distributed with mean of zero and standard deviation of 5% of the ancestral $P(T)$ value), community function improved at a slower rate than zero measurement uncertainty (compare Figure S16 left panel with Figure 5 J & K). When measurement uncertainty doubled, community selection failed (Figure S16 right panels). Thus, multiple measurements to reduce measurement uncertainty can make community selection more effective.

Robust conclusions under alternative model assumptions

We have demonstrated that during selection for high H-M community function, seemingly innocuous experimental procedures (e.g. pipetting) could be problematic, and more precise procedures might be required. Our conclusions hold when we used a much lower mutation rate (2×10^{-5} instead of 2×10^{-3} mutation per cell per generation per phenotype, Figure S17), although lower mutation rate slowed down community function improvement. Our conclusions also hold when we used a different distribution of mutation effects (a non-null mutation increased or decreased f_P by on average 2%, Figure S18), or incorporating epistasis (a non-null mutation would likely reduce f_P if the current f_P was high, and enhance f_P if the current f_P was low; Figure S19; Figure S20; Methods Section 5).

To further test the generality of our conclusions, we simulated community selection on a mutualistic H-M community. Specifically, we assumed that Byproduct was inhibitory to H. Thus, H benefited

M by providing Byproduct, and M benefited H by removing the inhibitory Byproduct, similar to the syntrophic community of *Desulfovibrio vulgaris* and *Methanococcus maripaludis* [51]. We obtained similar conclusions in this mutualistic H-M community (Figure S22).

Community selection can enforce species coexistence

In most communities, species coexistence may not be guaranteed due to competition for shared resources. Here, we show that properly executed community selection could also improve the functions of such communities, in part by forcing species coexistence. Consider an H-M community where H had the evolutionary potential to grow much faster than M. In this case, high community function not only required M to pay a fitness cost of f_P, but also required H to grow sufficiently slowly to not out-compete M. When community selection was ineffective ("pipetting"; Figure 7A), H's maximal growth rate evolved to exceed M's maximal growth rate (Figure S21A, compare i and iv). This drove M to almost extinction, and community function was very low (Figure 7A; Figure S21A, vi). During effective community selection (fixing H and M's biomass in Newborns; Figure 7B), H's maximal growth rate remained far below its evolutionary upper bound, and H's affinity for Resource even decreased from its ancestral value (Figure S21B, iv and v). In this case, H and M can coexist at a moderate ratio, and community function improved (Figure 7B).

In summary, our conclusions seem general under a variety of model assumptions and apply to a variety of communities.

Discussions

How might we improve functions of multi-species microbial communities via artificial selection? A common approach is to identify appropriate combinations of species types [8, 9, 12, 11, 15]. However, if we solely rely on species types, then without a constant influx of new species, community function will likely level off quickly [10]. Here, we consider artificial selection of communities with defined member species so that improvement of community function requires new genotypes that contribute more toward the community function at a cost to itself.

Artificial selection of whole communities to improve a costly community function requires careful considerations. These considerations include the definition of community function (Methods, Section 7), species choice (Figures 3 and 4), mutation rate, the total number of communities under selection, Newborn target total biomass (Figure S8), the number of generations during maturation (which in turn depends on the amount of Resource added to each Newborn and the maturation time; Figure S8), how we reproduce a selected Adult (e.g. volumetric dilution versus cell sorting, Figure 5), and the uncertainty in community function measurements (Figure S16).

Some of these considerations concern the heredity of the community function under selection. If a community function is highly sensitive to species biomass in Newborn communities, such as $P(T)$ of the H-M community, community selection faces a dilemma: On the one hand, a large Newborn size (BM_{target}) would lead to reproducible take-over by non-producers (Figure S8). On the other hand, a small Newborn size means that large non-heritable variations in community function can readily arise (e.g. during pipetting) and interfere with selection (Figure 5A-C). In this case, suppressing such non-heritable variations (e.g. sorting a fixed biomass or a fixed cell number of each species into Newborns) was critical to successful community selection (Figure 5J-L; Figure S15). Similar conclusions hold when we varied model assumptions (Results).

In the work of [8], authors tested two selection regimens with Newborn sizes differing by 100-fold. The authors hypothesized that smaller Newborns would have a high level of variation which should facilitate selection. However, the hypothesis was not corroborated by experiments. As a possible explanation, the authors invoked the "butterfly effect" (the sensitivity of chaotic systems to initial conditions). Our results suggest that even for non-chaotic systems like the H-M community, selection could fail due to interference from non-heritable variations. This is because in Newborns with small sizes, fluctuations in community composition can be large, which compromises heredity of community trait.

In certain regards, community selection is similar to selection of mono-species groups. Group selection, and in a related sense, kin selection [35, 36, 37, 38, 39, 40, 41, 42, 43, 44, 45, 46, 47, 48, 49], have been extensively examined to explain, for example, the evolution of traits that lower individual fitness but increase the success of a group (e.g. sterile ants) [1]. In both group selection and community selection, Newborn size must not be too large [57, 58] and maturation time must not be too long. Otherwise, all entities (groups or communities) will accumulate non-contributors in a similar fashion, and this low inter-entity variation impedes selection (Price equation [59]; Figure S1B; Figure S8).

Community selection and group selection do differ in other aspects. First, species interactions in a community could drive species composition to a value sub-optimal for community function ([60]). This problem does not exist for group selection especially when a group does not differentiate into interacting subgroups. Second, in group selection, when a Newborn group starts with a small number of individuals (e.g. one individual), a fraction of Newborn groups of the next cycle will be highly similar to the original Newborn group (Figure S1B, bottom panel). This facilitates group selection. In contrast, when a Newborn community starts with a small number of total individuals, large stochastic fluctuations in Newborn composition can interfere with community selection (Figure 5). In the extreme case, a member species may even be lost by chance. Even if a fixed biomass of each species is sorted into Newborns, heredity is much reduced during community selection due to random sampling of genotypes from member species [2].

Community function may not be maximized through pre-optimizing member species in monocultures. This is due to the difficulty of recapitulating community dynamics in monocultures. For example, we could start with H and M with all growth parameters at respective upper bounds (similar to Figure 5), and then improve M's f_P by mono-species group selection (Figure S1B). Specifically, we could start with n_{tot} of 100 Newborn M groups, each inoculated with one M cell (to facilitate group selection, Figure S1B bottom panel) [57]. We would supply each Newborn M group with the same amount of Resource as we would for H-M communities and excess Byproduct (since it is difficult to reproduce community Byproduct dynamics in M groups) [3]. After incubating these M groups for the same maturation time T, the group with the highest level of Product, $P(T)$, would be selected and reproduced into Newborn M groups for the next cycle. Optimal f_P for monoculture $P(T)$ occurred at an intermediate value ($f^*_{P,Mono} = 0.13$; Figure S23; Figure S24). However, optimal f_P for monoculture $P(T)$ is much lower

[1] Group selection is often applied in a broader sense to spatially-structured populations to explain the evolution of cooperative traits [52, 53]. In these cases, individuals form groups. Within each cycle, individuals grow based on their genotype (e.g. cooperators or cheaters) and group environment (cooperator-dominated or cheater-dominated). At the end of each cycle, individuals migrate among groups. However, if there are no births or deaths of groups, then selection acts on individuals instead of on groups [54, 55, 56].

[2] For example, if Newborn groups are initiated with a single contributor and if the highest-functioning Adult group has accumulated 50% non-contributors, then 50% Newborns of the next cycle will be initiated with a single contributor. In contrast, if a Newborn community starts with one contributor from each of the two species and if the highest-functioning Adult has accumulated 50% non-contributors in each species, then only 50%$\times$50%= 25% Newborns of the next cycle will be initiated with pure contributors.

[3] Since Newborn groups start with a single M individual, artificial group selection here can also be viewed as artificial individual selection where the trait under selection is an individual M's ability to make Product over time T as the individual grows into a population.

than optimal f_P for community $P(T)$ (Figure S23; see Methods Section 8 for an explanation). Thus, optimizing monoculture activity does not necessarily lead to optimized community function.

A general ramification of our work is that before launching a selection experiment, one should carefully consider the selection regimen. Although some community functions are not sensitive to fluctuations in Newborn biomass compositions (e.g. steady state ratio or growth rate of mutualistic communities [61, 33]), many are. How might we check? In the first method, one could initiate Newborn community replicates and measure community functions using the most precise method (e.g. cell sorting during Newborn formation; many repeated measurements of community function). Despite this, some levels of non-heritable variations in community function are inevitable due to, for example, non-genetic phenotypic variations among cells [62] or stochasticity in cell birth and death. If "noises" (variations among community replicates) are small compared to "signals" (variations among communities with different genotypes and thus different community functions), then one can test and possibly adopt less precise procedures (e.g. cell culture pipetting during Newborn formation; fewer repeated measurements of community function). In the second method, if significant variations in community function naturally arise within the first few cycles, one could experimentally evaluate whether community functions of the previous cycle (Figure 6A, bottom row) are correlated with community functions of the current cycle (Figure 6A, top row) across independent lineages.

Microbes can co-evolve with each other and with their host in nature [63, 64, 65]. Some have proposed that complex microbial communities such as the gut microbiota could serve as a unit of selection [14]. Our work suggests that if selection for a costly microbial community function should occur in nature, then mechanisms for suppressing non-heritable variations in community function should be in place.

Methods

1 Equations

H, the biomass of H, changes as a function of growth and death,

$$\frac{dH}{dt} = g_H(\hat{R})H - \delta_H H \tag{1}$$

Grow rate g_H depends on the level of Resource $\hat{R}$ (hat $\hat{}$ representing pre-scaled value) as described by the Monod growth model

$$g_H(\hat{R}) = g_{Hmax}\frac{\hat{R}}{\hat{R} + \hat{K}_{HR}}$$

where $\hat{K}_{HR}$ is the $\hat{R}$ at which $g_{Hmax}/2$ is achieved. δ_H is the death rate of H. Note that since Waste is in excess, Waste level does not change and thus does not enter the equation.

M, the biomass of M, changes as a function of growth and death,

$$\frac{dM}{dt} = (1 - f_P)\, g_M(\hat{R},\, \hat{B})M - \delta_M M \tag{2}$$

Total potential growth rate of M g_M depends on the levels of Resource and Byproduct ($\hat{R}$ and $\hat{B}$) according to the Mankad-Bungay model [23] due to its experimental support:

$$g_M(\hat{R},\, \hat{B}) = g_{Mmax}\frac{\hat{R}_M\hat{B}_M}{\hat{R}_M + \hat{B}_M}\left(\frac{1}{\hat{R}_M + 1} + \frac{1}{\hat{B}_M + 1}\right)$$

where $\hat{R}_M = \hat{R}/\hat{K}_{MR}$ and $\hat{B}_M = \hat{B}/\hat{K}_{MB}$ (Figure S3). $1 - f_P$ fraction of M growth is channeled to biomass increase. f_P fraction of M growth is channeled to making Product:

$$\frac{d\hat{P}}{dt} = \tilde{r}_P f_P g_M(\hat{R},\, \hat{B})M \tag{3}$$

where $\tilde{r}_P$ is the amount of Product made at the cost of one M biomass (tilde $\sim$ representing scaling factor, see below and Table 1).

Resource $\hat{R}$ is consumed proportionally to the growth of M and H; Byproduct $\hat{B}$ is released proportionally to H growth and consumed proportionally to M growth:

$$\frac{d\hat{R}}{dt} = -\hat{c}_{RM} g_M(\hat{R},\, \hat{B})M - \hat{c}_{RH} g_H(\hat{R})H \tag{4}$$

$$\frac{d\hat{B}}{dt} = \tilde{r}_B g_H(\hat{R})H - \hat{c}_{BM} g_M(\hat{R},\, \hat{B})M \tag{5}$$

Here, $\hat{c}_{RM}$ and $\hat{c}_{RH}$ are the amounts of $\hat{R}$ consumed per potential M biomass and H biomass, respectively. $\hat{c}_{BM}$ is the amount of $\hat{B}$ consumed per potential M biomass. $\tilde{r}_B$ is the amount of $\hat{B}$ released per H biomass grown. Our model assumes that Byproduct or Product is generated proportionally to H or M biomass grown, which is reasonable given the stoichiometry of metabolic reactions and experimental support [66]. The volume of community is set to be 1, and thus cell or metabolite quantities (which are considered here) are numerically identical to cell or metabolite concentrations.

In equations above, scaling factors are marked by "$\sim$", and will become 1 after scaling. Variables and parameters with hats will be scaled and lose their hats afterwards. Variables and parameters without hats will not be scaled. We scale Resource-related variable ($\hat{R}$) and parameters ($\hat{K}_{MR}$, $\hat{K}_{HR}$, $\hat{c}_{RM}$, and $\hat{c}_{RH}$) against $\tilde{R}(0)$ (Resource supplied to Newborn), Byproduct-related variable ($\hat{B}$) and parameters ($\hat{K}_{MB}$ and $\hat{c}_{BM}$) against $\tilde{r}_B$ (amount of Byproduct released per H biomass grown), and Product-related variable ($\hat{P}$) against $\tilde{r}_P$ (amount of Product made at the cost of one M biomass). For biologists who usually think of quantities with units, the purpose of scaling (and getting rid of units) is to reduce the number of parameters. For example, H biomass growth rate can be re-written as:

$$\begin{aligned} g_H(\hat{R}) &= g_{Hmax}\frac{\hat{R}}{\hat{R} + \hat{K}_{HR}} \\ &= g_{Hmax}\left(\frac{\hat{R}}{\tilde{R}(0)}\right) \Big/ \left(\frac{\hat{R}}{\tilde{R}(0)} + \frac{\hat{K}_{HR}}{\tilde{R}(0)}\right) \\ &= g_{Hmax}\frac{R}{(R + K_{HR})} \\ &= g_H(R) \end{aligned}$$

where $R = \hat{R}/\tilde{R}(0)$ and $K_{HR} = \hat{K}_{HR}/\tilde{R}(0)$. Thus, the unscaled $g_H(\hat{R})$ and the scaled $g_H(R)$ share identical forms (Figure S3). After scaling, the value of $\tilde{R}(0)$ becomes irrelevant (1 with no unit). Similarly, since $\hat{R}_M = \frac{\hat{R}}{\tilde{R}(0)} \Big/ \frac{\hat{K}_{MR}}{\tilde{R}(0)} = \frac{R}{K_{MR}} = R_M$ and $\hat{B}_M = \frac{\hat{B}}{\tilde{r}_B} \Big/ \frac{\hat{K}_{MB}}{\tilde{r}_B} = \frac{B}{K_{MB}} = B_M$, $g_M(\hat{R},\, \hat{B}) = g_M(R,\, B)$ (Figure S4).

Thus, scaled equations are

$$\frac{dH}{dt} = g_H(R)H - \delta_H H \tag{6}$$

$$\frac{dM}{dt} = (1 - f_P)\, g_M(R,\, B)M - \delta_M M \tag{7}$$

$$\begin{aligned} \frac{dP}{dt} &= \frac{d\hat{P}}{\widetilde{r}_P dt} \\ &= f_P g_M(\hat{R},\, \hat{B})M \\ &= f_P g_M(R,\, B)M \end{aligned} \tag{8}$$

$$\begin{aligned} \frac{dR}{dt} &= \frac{d\hat{R}/\widetilde{R}(0)}{dt} \\ &= -\frac{\hat{c}_{RM}}{\widetilde{R}(0)} g_M(\hat{R},\, \hat{B})M - \frac{\hat{c}_{RH}}{\widetilde{R}(0)} g_H(\hat{R})H \\ &= -c_{RM} g_M(R,\, B)M - c_{RH} g_H(R)H \end{aligned} \tag{9}$$

$$\begin{aligned} \frac{dB}{dt} &= \frac{d\hat{B}/\widetilde{r}_B}{dt} \\ &= g_H(\hat{R})H - \frac{\hat{c}_{BM}}{\widetilde{r}_B} g_M(\hat{R},\, \hat{B})M \\ &= g_H(R)H - c_{BM} g_M(R,\, B)M \end{aligned} \tag{10}$$

We have not scaled time here, although time can also be scaled by, for example, the community maturation time. Here, time has the unit of unit time (e.g. hr), and to avoid repetition, we often drop the time unit. After scaling, values of all parameters (including scaling factors) are in Table 1, and variables in our model and simulations are summarized in Table 2.

From Eq. 10:

$$\int_0^T \frac{dB}{dt} dt = \int_0^T g_H(R)H dt - \int_0^T c_{BM} g_M(R,\, B)M dt. \tag{11}$$

If we approximate Eq. 6-7 by ignoring the death rates so that $\frac{dH}{dt} \approx g_H(R)H$ and $\frac{dM}{dt} \approx (1 - f_P)\, g_M(R,\, B)M$, Eq. 11 becomes

$$B(T) \approx \int_0^T \frac{dH}{dt} dt - \frac{c_{BM}}{1 - f_P} \int_0^T \frac{dM}{dt} dt. \tag{12}$$

If B is the limiting factor for the growth of M so that B is mostly depleted, we can approximate $B \approx 0$. If T is large enough so that both M and H has multiplied significantly and $H(T) \gg H(0)$ and $M(T) \gg M(0)$, Eq. 12 becomes

$$H(T) - H(0) - \frac{c_{BM}}{1 - f_P} (M(T) - M(0)) \approx H(T) - \frac{c_{BM}}{1 - f_P} M(T) \approx 0,$$

the M:H ratio at time T is

$$\frac{M(T)}{H(T)} \approx \frac{1 - f_P}{c_{BM}}. \tag{13}$$

	Definition	Ancestral	Evolved
$\widetilde{r}_B$	amount of $\hat{B}$ released per H biomass grown	scaling factor, 1	no change
$\widetilde{r}_P$	amount of $\hat{P}$ released at the cost of one M biomass	scaling factor, 1	no change
$\widetilde{R}(0)$	initial amount of Resource in Newborn	scaling factor, 1	
f_P	fraction of M growth diverted to producing P	0.10	0.13#
K_{MR}	fold of $\widetilde{R}(0)$ at which $g_{Mmax}/2$ is achieved in excess B	1	$1/3$*
K_{MB}	amount of $\hat{B}$ at which $g_{Mmax}/2$ is achieved in excess R, scaled against $\widetilde{r}_B$	$\frac{5}{3} \times 10^2$	$\frac{1}{3} \times 10^2$*
K_{HR}	fold of $\widetilde{R}(0)$ at which $g_{Hmax}/2$ is achieved	1	$1/5$*
g_{Mmax}	maximal biomass growth rate of M	0.58/unit time	0.7/unit time*
g_{Hmax}	maximal biomass growth rate of H	0.25/unit time	0.3/unit time*
δ_M	death rate of M	3.5×10^{-3}/unit time	no change
δ_H	death rate of H	1.5×10^{-3}/unit time	no change
c_{RM}	fraction of $\widetilde{R}(0)$ consumed per M biomass grown	10^{-4}	no change
c_{RH}	fraction of $\widetilde{R}(0)$ consumed per H biomass grown	10^{-4}	no change
c_{BM}	amount of $\hat{B}$ consumed per M biomass grown, scaled against $\widetilde{r}_B$	$\frac{1}{3}$	no change
P_{mut}	mutation probability per cell division for each mutable phenotype	$2 \times 10^{-5} \sim 2 \times 10^{-3}$	

Table 1: Parameters for ancestral and evolved (growth- and mono-adapted) H and M. Parameters in the "Evolved" column are used for most simulations and figures unless otherwise specified. For maximal growth rates, * represents evolutionary upper bound. For $K_{SpeciesMetabolite}$, * represents evolutionary lower bound, which corresponds to evolutionary upper bound for Species's affinity for Metabolite ($1/K_{SpeciesMetabolite}$). # is from Figure S23. In Methods Section 2, we explained our parameter choices (including why we hold some parameters constant during evolution).

The steady state ϕ_M, $\phi_{M,SS}$, is then

$$\phi_{M,SS} \approx \frac{1 - f_P}{1 - f_P + c_{BM}}, \tag{14}$$

because if a community has $\phi_M(0) = \phi_{M,SS}$ at its Newborn stage, it has the same $\phi_M(T) = \phi_{M,SS}$ at its Adult stage.

In our simulations, because we supplied the H-M community with abundant R to avoid stationary phase, H grows almost at the maximal rate through T and releases B. If f_P is not too large ($f_P < 0.4$), which is satisfied in our simulations, M grows at a maximal rate allowed by B and keeps B at a low level. Thus, Eq. 14 is applicable and predicts the steady-state $\phi_{M,SS}$ well (see Figure S25). Note that significant deviation occurs when $f_P > 0.4$. This is because when f_P is large, M's biomass does not grow fast enough to deplete B so that we cannot approximate $B(T) \approx 0$ anymore.

2 Parameter choices

Our parameter choices are based on experimental measurements from a variety of organisms. Additionally, we chose growth parameters (maximal growth rates and affinities for metabolites) of ancestral and evolved H and M so that 1) the two species can coexist at a moderate ratio for a range of f_P over multiple

Symbols	Definition
T	Community maturation time, corresponding to the duration of a selection cycle
t	Time within a selection cycle, $0 \leq t \leq T$
$M(t)$, $H(t)$	The biomass of M or H in a community at time t
$BM(t) = M(t) + H(t)$	The total biomass in a community at time t
$\phi_M(t)$	The fraction of M biomass at time t
BM_{target}	Pre-set target total biomass of Newborns during community reproduction
$I_M(t)$, $I_H(t)$	The integer number of M or H cells in a community at time t
$\varphi_M(t)$	The fraction of M individuals at time t
$L_M(t)$, $L_H(t)$	The biomass (length) of an individual M or H cell at time t, $1 \leq L_M(t)$, $L_H(t) \leq 2$
$\overline{L}$	The average biomass (length) of an individual M or H cell.
$P(t)$	The amount of Product P in a community at time t, scaled by $\widetilde{r}_P$
$R(t)$	The amount of Resource R in a community at time t, scaled by $\widetilde{R}(0)$
$B(t)$	The amount of Byproduct B in a community at time t, scaled by $\widetilde{r}_B$
n_{dil}	The fold dilution when reproducing an Adult community
n_{tot}	Total number of communities under selection in each cycle

Table 2: A summary of variables used in the simulation.

selection cycles and 2) improving all growth parameters up to their evolutionary upper bounds generally improves community function (Methods Section 3). This way, we could simplify our simulation by fixing growth parameters at their respective evolutionary upper bounds. With only one mutable parameter (f_P), we can identify the optimal f_P^* associated with maximal community function (Figure **??**).

For ancestral H, we set $g_{Hmax} = 0.25$ (equivalent to 2.8-hr doubling time if we choose hr as the time unit), $K_{HR} = 1$ and $c_{RH} = 10^{-4}$ (both with unit of $\widetilde{R}(0)$) (Table 1). This way, ancestral H can grow by about 10-fold by the end of $T = 17$. These parameters are biologically realistic. For example, for a *lys-S. cerevisiae* strain with lysine as Resource, un-scaled Monod constant is $\hat{K} = 1$ μM, and consumption $\hat{c}$ is 2 fmole/cell (Ref. [34], Figure 2 Source Data 1, bioRxiv). Thus, if we choose 10 μL as the community volume $\hat{V}$ and 2 μM as the initial Resource concentration, then $\widetilde{R}(0) = 2 \times 10^4$ fmole. After scaling, $K = \hat{K}\hat{V}/\widetilde{R}(0) = 0.5$ and $c = \hat{c}/\widetilde{R}(0) = 10^{-4}$, comparable to values in Table 1.

To ensure the coexistence of H and M, M must grow faster than H for part of the maturation cycle. Since we have assumed M and H to have the same affinity for R (Table 1), g_{Mmax} must exceed g_{Hmax} (Figure 1), and M's affinity for Byproduct ($1/K_{MB}$) must be sufficiently large. Moreover, metabolite release and consumption need to be balanced to avoid extreme ratios between metabolite releaser and consumer. Thus for ancestral M, we chose $g_{Mmax} = 0.58$ (equivalent to a doubling time of 1.2 hrs). We set $c_{BM} = \frac{1}{3}$ (units of $\widetilde{r}_B$), meaning that Byproduct released during one H biomass growth is sufficient to generate 3 potential M biomass, which is biologically achievable ([33, 67]). When we chose $K_{MB} = \frac{5}{3} \times 10^2$ (units of $\widetilde{r}_B$), H and M can coexist for a range of f_P (Figure 3). This value is biologically realistic. For example, suppose that H releases hypoxanthine as Byproduct. A hypoxanthine-requiring *S. cerevisiae* M strain evolved under hypoxanthine limitation could achieve a Monod constant for hypoxanthine at 0.1 μM (bioRxiv). If the volume of the community is 10 μL, then $K_{MB} = \frac{5}{3} \times 10^2$ (units of $\widetilde{r}_B$) corresponds to an absolute release rate $\widetilde{r}_B = 0.1\,\mu M \times 10\mu\text{L}/(\frac{5}{3} \times 10^2) = 6$ fmole per releaser biomass born. At 8 hour doubling time, this translates to 6 fmole/(1 cell$\times$8 hr)≈ 0.75 fmole/cell/hr, within the ballpark of experimental observation (~0.3 fmole/cell/hr, bioRxiv). As a comparison, a lysine-overproducing yeast strain reaches a release rate of 0.8 fmole/cell/hr (bioRxiv) and a leucine-overproducing strain reaches a release rate of 4.2 fmole/cell/hr ([67]). Death rates δ_H and δ_M were

chosen to be 0.5% of H and M's respective upper bound of maximal growth rate, which are within the ballpark of experimental observations (e.g. the death rate of a *lys-* strain in lysine-limited chemostat is 0.4% of maximal growth rate, bioRxiv).

We assume that H and M consume the same amount of R per new cell ($c_{RH} = c_{RM}$) since the biomass of various microbes share similar elemental (e.g. carbon or nitrogen) compositions [68]. Specifically, $c_{RH} = c_{RM} = 10^{-4}$ (units of $\widetilde{R}(0)$), meaning that the Resource supplied to each Newborn community can yield a maximum of 10^4 total biomass.

In simulations shown in Figures 4B, S9, S10, S13, growth parameters (maximal growth rates g_{Mmax} and g_{Hmax} and affinities for nutrients $1/K_{MR}$, $1/K_{MB}$, and $1/K_{HR}$) and production cost parameter ($0 \leq f_P \leq 1$) were allowed to change from ancestral values during community maturation, since these phenotypes have been observed to rapidly evolve within tens to hundreds of generations ([25, 26, 27, 28]). For example, several-fold improvement in nutrient affinity and ~20% increase in maximal growth rate have been observed in experimental evolution [28, 26]. We therefore allowed affinities $1/K_{MR}$, $1/K_{HR}$, and $1/K_{MB}$ to increase by up to 3-fold, 5-fold, and 5-fold respectively, and allowed g_{Hmax} and g_{Mmax} to increase by up to 20%. These bounds also ensured that evolved H and M could coexist for $f_p < 0.5$, and that Resource was on average not depleted by T to avoid cells entering stationary phase.

We also simulated community selection where improved growth parameters could reduce community function (Figure 4A). In this simulation, g_{Hmax} was allowed to increase by up to 220% and each Newborn community was supplied with R that can support up to 10^5 cells (10 units of $\widetilde{R}(0)$).

Although maximal growth rate and nutrient affinity can sometimes show trade-off (e.g. Ref. [26]), for simplicity we assumed here that they are independent of each other. We held metabolite consumption (c_{RM}, c_{BM}, c_{RH}) constant because conversion of essential elements such as carbon and nitrogen into biomass is unlikely to evolve quickly and dramatically, especially when these elements are not in large excess ([68]). Similarly, we held the scaling factors $\widetilde{r}_P$ and $\widetilde{r}_B$ constant, assuming that they do not change rapidly during evolution due to stoichiometric constraints of biochemical reactions. We held death rates (δ_M, δ_H) constant because they are much smaller than growth rates in general and thus any changes are likely inconsequential.

3 Choosing growth parameter ranges so that we can fix growth parameters to upper bounds

Improving individual growth (maximal growth rate and affinity for metabolites) does not always lead to improved community function (Figure 4A). However, we have chosen H and M growth parameters so that improving them from their ancestral values up to upper bounds generally improves community function (see below). When Newborn communities are assembled from "growth-adapted" H and M with growth parameters at upper bounds, two advantages are apparent.

First, after fixing growth parameters of H and M to their upper bounds, we can identify a locally maximal community function. Specifically, for a Newborn with total biomass $BM(0) = 100$ and fixed Resource R, we can calculate $P(T)$ under various f_P and $\phi_M(0)$, assuming that all M cells have the same f_P. Since both numbers range between 0 and 1, we calculate $P(T,\, f_P = 0.01 \times i,\, \phi_M(0) = 0.01 \times j)$ for integers i and j between 1 and 99. There is a single maximum for $P(T)$ when $i = 41$ and $j = 54$. In other words, if M invests $f_P^* = 0.41$ of its potential growth to make Product and if the fraction of M biomass in Newborn $\phi_M^*(0) = 0.54$, then maximal community function $P^*(T)$ is achieved (Figure **??**A; magenta dashed line in Figure 5).

Second, growth-adapted H and M are evolutionarily stable in the sense that deviations (reductions) from upper bounds will reduce both individual fitness and community function, and are therefore disfa-

vored by natural selection and artificial selection on the community function.

Below, we present evidence that within our parameter ranges (Table 1), improving growth parameters generally improves community function. When f_P is optimal for community function ($f_P^* = 0.41$), if we fix four of the five growth parameters to their upper bounds, then as the remaining growth parameter improves, community function increases (magenta lines in top panels of Figure S26). Moreover, mutants with a reduced growth parameter are out-competed by their growth-adapted counterparts (magenta lines in bottom panels of Figure S26).

When $f_P = f^*_{P,\,Mono} = 0.13$ (optimal for M-monoculture function in Figure S23; the starting genotype for most community selection trials in this paper), community function and individual fitness generally increase as growth parameters improve (black dashed lines in Figure S26). However, when M's affinity for Resource ($1/K_{MR}$) is reduced from upper bound, fitness improves slightly (black dashed line in Panel J, Figure S26). Mathematically speaking, this is a consequence of the Mankad-Bungay model [23] (Figure S4B). Let $R_M = R/K_{MR}$ and $B_M = B/K_{MB}$. Then,

$$\begin{aligned}
\frac{\partial g_M}{\partial K_{MR}} &= \frac{\partial g}{\partial R_M}\frac{\partial R_M}{\partial K_{MR}} = \frac{\partial\left[g_{max}\frac{R_M B_M}{R_M+B_M}\left(\frac{1}{1+R_M}+\frac{1}{1+B_M}\right)\right]}{\partial R_M}\frac{\partial R_M}{\partial K_{MR}} \\
&= g_{max}\frac{-R_M}{K_{MR}}\left[\frac{B_M\left(R_M+B_M\right)-R_M B_M}{\left(R_M+B_M\right)^2}\left(\frac{1}{1+R_M}+\frac{1}{1+B_M}\right)-\frac{R_M B_M}{R_M+B_M}\frac{1}{\left(1+R_M\right)^2}\right] \\
&= g_{max}\frac{R_M B_M}{\left(R_M+B_M\right)K_{MR}}\left(\frac{R_M}{(1+R_M)^2}-\frac{B_M}{R_M+B_M}\left(\frac{1}{1+R_M}+\frac{1}{1+B_M}\right)\right)
\end{aligned}$$

If $R_M \ll 1 \ll B_M$ (corresponding to limiting R and abundant B),

$$\frac{R_M}{(1+R_M)^2}-\frac{B_M}{R_M+B_M}\left(\frac{1}{1+R_M}+\frac{1}{1+B_M}\right) \approx \frac{R_M}{(1+R_M)^2}-\frac{1}{1+R_M} = -\frac{1}{(1+R_M)^2} \tag{15}$$

and thus $\frac{\partial g_M}{\partial K_{MR}} < 0$. This is the familiar case where growth rate increases as the Monod constant decreases (i.e. affinity increases). However, if $B_M \ll 1 \ll R_M$

$$\frac{R_M}{(1+R_M)^2}-\frac{B_M}{R_M+B_M}\left(\frac{1}{1+R_M}+\frac{1}{1+B_M}\right) \approx \frac{1}{R_M}-\frac{B_M}{R_M}\left(\frac{1}{1+B_M}\right) = \frac{1}{R_M(1+B_M)} \tag{16}$$

and thus $\frac{\partial g_M}{\partial K_{MR}} > 0$. In this case, growth rate decreases as the Monod constant decreases (i.e. affinity increases). In other words, decreased affinity for the abundant nutrient improves growth rate. Transporter competition for membrane space [69] could lead to this result, since reduced affinity for abundant nutrient may increase affinity for rare nutrient. At the beginning of each cycle, R is abundant and B is limiting (Eq. 16). Therefore M cells with lower affinity for R will grow faster than those with higher affinity (Figure S27). At the end of each cycle, the opposite is true (Figure S27). As f_P decreases, M diverts more toward biomass growth and the first stage of B limitation lasts longer. Consequently, M can gain a slightly higher overall fitness by lowering the affinity for R (Figure S27A).

Regardless, decreased M affinity for Resource ($1/K_{MR}$) only leads to a very slight increase in M fitness (Figure S26J) and a very slight decrease in $P(T)$ (Figure S27B). Moreover, this only occurs at low f_P at the beginning of community selection, and thus may be neglected. Indeed, if we start all growth parameters at their upper bounds and $f_P = 0.13$, and perform community selection while allowing all parameters to vary (Figure S28), then $1/K_{MR}$ decreases somewhat, yet the dynamics of f_P is similar to when we only allow f_P to change (compare Figure S28D with Figure 5A).

4 Mutation rate and the distribution of mutation effects

Literature values of mutation rate and the distribution of mutation effects are highly variable. Below, we briefly review the literature and discuss rationales of our choices.

Among mutations, a fraction is neutral in that they do not affect the phenotype of interest. For example, the vast majority of synonymous mutations are neutral [70]. Furthermore, mutations wtih small effects may appear neutral, which can depend on the effective population size and selection condition. For example, at low population size due to genetic drift (i.e. changes in allele frequencies due to chance), a beneficial or deleterious mutation may not be selected for or selected against, and is thus neutral with respect to selection [71, 72]. As another example, the same mutation in an antibiotic-degrading gene can be neutral under low antibiotic concentrations, but deleterious under high antibiotic concentrations [73]. We term all these cases as "neutral" mutations.

Since a larger fraction of neutral mutations is equivalent to a lower rate of phenotype-altering mutations, our simulations define "mutation rate" as the rate of non-neutral mutations that either enhance a phenotype ("enhancing mutations") or diminish a phenotype ("diminishing mutations"). Enhancing mutations of maximal growth rates (g_{Hmax} and g_{Mmax}) and of nutrient affinities ($1/K_{HR}$, $1/K_{MR}$, $1/K_{MB}$) enhance the fitness of an individual ("beneficial mutations"). In contrast, enhancing mutations in f_p diminish the fitness of an individual ("deleterious mutations").

Depending on the phenotype, the rate of phenotype-altering mutations is highly variable. Although mutations that cause qualitative phenotypic changes (e.g. drug resistance) occur at a rate of 10^{-8}~10^{-6} per genome per generation in bacteria and yeast [74, 75], mutations affecting quantitative traits such as growth rate occur much more frequently. For example in yeast, mutations that increase growth rate by $\geq 2\%$ occur at a rate of $\sim 10^{-4}$ per genome per generation (calculated from Figure 3 of Ref. [76]), and mutations that reduce growth rate occur at a rate of $10^{-4} \sim 10^{-3}$ per genome per generation [31, 77]. Moreover, mutation rate can be elevated by as much as 100-fold in hyper-mutators where DNA repair is dysfunctional [78, 79, 77]. In our simulations, we assume a high, but biologically feasible, rate of 2×10^{-3} phenotype-altering mutations per cell per generation per phenotype to speed up computation. At this rate, an average community would sample ~20 new mutations per phenotype during maturation. We have also simulated with a 100-fold lower mutation rate. As expected, evolutionary dynamics slowed down, but all of our conclusions still held (Figure S17).

Among phenotype-altering mutations, tens of percent create null mutants, as illustrated by experimental studies on protein, viruses, and yeast [29, 30, 31]. Thus, we assumed that 50% of phenotype-altering mutations were null (i.e. resulting in zero maximal growth rate, zero affinity for metabolite, or zero f_P). Among non-null mutations, the relative abundances of enhancing versus diminishing mutations are highly variable in different experiments. It can be impacted by effective population size. For example, with a large effective population size, the survival rate of beneficial mutations is 1000-fold lower due to clonal interference (competition between beneficial mutations) [80]. The relative abundance of enhancing versus diminishing mutations also strongly depends on the starting phenotype [29, 73, 71]. For example with ampicillin as a substrate, the wild-type TEM-1 β-lactamase is a "perfect" enzyme. Consequently, mutations were either neutral or diminishing, and few enhanced enzyme activity [73]. In contrast with a novel substrate such as cefotaxime, the enzyme had undetectable activity, and diminishing mutations were not detected while 2% of tested mutations were enhancing [73]. When modeling H-M communities, we assumed that the ancestral H and M had intermediate phenotypes that can be enhanced or diminished.

We based our distribution of mutation effects on experimental studies where a large number of enhancing and diminishing mutants have been quantified in an unbiased fashion. An example is a study from the Dunham lab where the fitness effects of thousands of *S. cerevisiae* mutations were quantified

under various nutrient limitations [32]. Specifically for each nutrient limitation, the authors first measured $\triangle s_{WT} = (w_{WT} - \bar{w}_{WT})/\bar{w}_{WT} = w_{WT}/\bar{w}_{WT} - 1$, the deviation in relative fitness of thousands of bar-coded wild-type control strains from the wild-type mean fitness (i.e. selection coefficients). Due to experimental noise, $\triangle s_{WT}$ is distributed with zero mean and non-zero variance. Then, the authors measured thousands of $\triangle s_{MT}$, each corresponding to the relative fitness change of a bar-coded mutant strain with respect to the mean of wild-type fitness (i.e. $\triangle s_{MT} = (w_{MT} - \bar{w}_{WT})/\bar{w}_{WT}$). From these two distributions, we derived $\mu_{\Delta s}$, the probability density function (PDF) of relative fitness change caused by mutations $\Delta s = \triangle s_{MT} - \triangle s_{WT}$ (see Figure S6 for interpreting PDF), in the following manner.

First, we calculated $\mu_m(\triangle s_{MT})$, the discrete PDF of the relative fitness change of mutant strains, with bin width 0.04. In other words, $\mu_m(\triangle s_{MT})$ =counts in the bin of $[\triangle s_{MT} - 0.02,\ \triangle s_{MT} + 0.02]$ / total counts/0.04 where $\triangle s_{MT}$ ranges from -0.6 and 0.6 which is sufficient to cover the range of experimental outcome. The Poissonian uncertainty of μ_m is $\delta\mu_m(\triangle s_{MT}) = \sqrt{\text{counts per bin}}$/total counts/0.04. Repeating this process for the wild-type collection, we obtained the PDF of the relative fitness change of wild-type strains $\mu_w(\triangle s_{WT})$. Next, from $\mu_w(\triangle s_{WT})$ and $\mu_m(\triangle s_{MT})$, we derived $\mu_{\Delta s}(\Delta s)$, the PDF of Δs with bin width 0.04:

$$\mu_{\Delta s}(\Delta s = i \times 0.04) = 0.04 \times \sum_{j=-\infty}^{+\infty} \mu_w(j \times 0.04)\mu_m\left((i+j) \times 0.04\right). \tag{17}$$

assuming that $\triangle s_{MT}$ and $\triangle s_{WT}$ are independent from each other. Here, i is an integer from -15 to 15. The uncertainty for $\mu_{\Delta s}$ was calculated by propagation of error. That is, if f is a function of x_i (i = 1, 2, ..., n), then s_f, the error of f, is $s_f^2 = \sum \left(\frac{\partial f}{\partial x_i} s_{x_i}\right)^2$, where s_{x_i} is the error or uncertainty of x_i. Thus,

$$\delta\mu_{\Delta s}(i) = 0.04 \times \sqrt{\sum_j \left[(\delta\mu_w(j)\mu_m(i+j))^2 + (\mu_w(j)\delta\mu_m(i+j))^2\right]} \tag{18}$$

where $\mu_w(j)$ is short-hand notation for $\mu_w(\triangle s_{WT} = j \times 0.04)$ and so on. Our calculated $\mu_{\Delta s}(\Delta s)$ with error bar of $\delta\mu_{\Delta s}$ is shown in Figure S6.

Our reanalysis demonstrated that distributions of mutation fitness effects $\mu_{\Delta s}(\Delta s)$ are largely conserved regardless of nutrient conditions and mutation types (Figure S6B). In all cases, the relative fitness changes caused by beneficial (fitness-enhancing) and deleterious (fitness-diminishing) mutations can be approximated by a bilateral exponential distribution with means s_+ and s_- for the positive and negative halves, respectively. After normalizing the total probability to 1, we have:

$$\mu_{\Delta s}(\Delta s) = \begin{cases} \frac{1}{s_+ + s_-(1-\exp(-1/s_-))} \exp(-\Delta s/s_+) & \text{if } \Delta s \geq 0 \\ \frac{1}{s_+ + s_-(1-\exp(-1/s_-))} \exp(\Delta s/s_-) & \text{if } -1 < \Delta s < 0 \end{cases} \tag{19}$$

We fitted the Dunham lab haploid data (since microbes are often haploid) to Eq. 19, using $\mu_{\Delta s}(i)/\delta\mu_{\Delta s}(i)$ as the weight for non-linear least squared regression (green lines in Figure S6B). We obtained $s_+ = 0.050 \pm 0.002$ and $s_- = 0.067 \pm 0.003$.

Interestingly, exponential distribution described the fitness effects of deleterious mutations in an RNA virus remarkably well [29]. Based on extreme value theory, the fitness effects of beneficial mutations were predicted to follow an exponential distribution [81, 82], which has gained experimental support from bacterium and virus [83, 84, 85] (although see [86, 76] for counter examples). Evolutionary models based on exponential distributions of fitness effects have shown good agreements with experimental data [80, 87].

We have also simulated smaller average mutational effects based on measurements of spontaneous or chemically-induced (instead of deletion) mutations. For example, the fitness effects of nonlethal

deleterious mutations in *S. cerevisiae* were mostly 1%∼5% [31], and the mean selection coefficient of beneficial mutations in *E. coli* was 1%∼2% [83, 80]. As an alternative, we also simulated with $s_+ = s_- = 0.02$, and obtained the same conclusions (Figure S18).

5 Modeling epistasis on f_P

Epistasis, where the effect of a new mutation depends on prior mutations ("genetic background"), is known to affect evolutionary dynamics. Epistatic effects have been quantified in various ways. Experiments on viruses, bacteria, yeast, and proteins have demonstrated that if two mutations were both deleterious or random, viable double mutants experienced epistatic effects that distributed nearly symmetrically around a value close to zero [88, 89, 90, 91, 92]. In other words, a significant fraction of mutation pairs show no epistasis, and a small fraction show positive or negative epistasis (i.e. a double mutant displays a stronger or weaker phenotype than expected from additive effects of the two single mutants). Epistasis between two beneficial mutations can vary from being predominantly negative [89] to being symmetrically distributed around zero [90]. Furthermore, a beneficial mutation tends to confer a lower beneficial effect if the background already has high fitness ("diminishing returns") [93, 90, 94].

A mathematical model by Wiser et al. incorporates diminishing-returns epistasis [87]. In this model, beneficial mutations of advantage s in the ancestral background are exponentially distributed with probability density function (PDF) $\alpha \exp(-\alpha s)$, where $1/\alpha > 0$ is the mean advantage. After a mutation with advantage s has occurred, the mean advantage of the next mutation would be reduced to $1/[\alpha(1+gs)]$, where $g > 0$ is the "diminishing returns parameter". Wiser et al. estimates $g \approx 6$. This model quantitatively explains the fitness dynamics of evolving *E. coli* populations.

Based on the above experimental and theoretical literature, we modeled epistasis on f_P in the following manner. Let the relative mutation effect on f_P be $\Delta f_P = (f_{P,mut} - f_P)/f_P$ (note $\Delta f_P \geq -1$). Then, $\mu(\Delta f_P,\ f_P)$, the PDF of Δf_P at the current f_P value, is described by a form similar to Eq. 19:

$$\mu(\Delta f_P,\ f_P) = \begin{cases} \frac{1}{s_+(f_P)+s_-(f_P)(1-\exp(-1/s_-(f_P)))} \exp(-\Delta f_P/s_+(f_P)) & \text{if } \Delta f_P \geq 0 \\ \frac{1}{s_+(f_P)+s_-(f_P)(1-\exp(-1/s_-(f_P)))} \exp(\Delta f_P/s_-(f_P)) & \text{if } -1 < \Delta f_P < 0 \end{cases} \tag{20}$$

Here, $s_+(f_P)$ and $s_-(f_P)$ are respectively the mean Δf_P for enhancing and diminishing mutations at current f_P. We assigned $s_+(f_P) = s_{+init}/(1 + g \times (f_P/f_{P,init} - 1))$, where $f_{P,init}$ is the f_P of the initial background in a community selection simulation ($f_{P,init} = f^*_{P,Mono} = 0.13$), s_{+init} is the mean enhancing Δf_P occurring in the initial background, and $0 < g < 1$ is the epistatic factor. Similarly, $s_-(f_P) = s_{-init} \times (1+g\times(f_P/f_{P,init}-1))$ is the mean $|\Delta f_P|$ for diminishing mutations at current f_P. In the initial background, since $f_P = f_{P,init}$, we have $s_+(f_P) = s_{+init}$ and $s_-(f_P) = s_{-init}$ ($s_{+init} = 0.050$ and $s_{-init} = 0.067$ in Figure S6). Consistent with the diminishing returns principle, for subsequent mutations that alter f_P, if current $f_P > f_{P,init}$, then a new enhancing mutation became less likely and its mean effect smaller, while a new diminishing mutation became more likely and its mean effect bigger (ensured by $g > 0$; Figure S19 right panel). Similarly, if current $f_P < f_{P,init}$, then a new enhancing mutation became more likely and its mean effect bigger, while a diminishing mutation became less likely and its mean effect smaller (ensured by $0 < g < 1$; Figure S19 left panel). In summary, our model captured not only diminishing- returns epistasis, but also our understanding of mutational effects on protein stability [71].

6 Simulation code of community selection

As described in the main text, our simulations tracked the biomass and phenotypes of individual cells as well as the amounts of Resource, Byproduct, and Product in each community throughout community selection. Cell biomass growth, cell division, and changes in chemical concentrations were calculated deterministically. Stochastic processes including cell death, mutation, and the partitioning of cells of a selected Adult community into Newborn communities were simulated using the Monte Carlo method.

Specifically, each simulation was initialized with a total of $n_{tot} = 100$ Newborn communities with identical configuration:

- each community had 100 total cells of biomass 1. Thus, total biomass $BM(0) = 100$.
- 40 cells were H. 60 cells were M with identical f_P. Thus, M biomass $M(0) = 60$ and fraction of M biomass $\phi_M(0) = 0.6$.

Our community selection simulations did not consider mutations arising during pre-growth prior to inoculating Newborns of the first cycle, because incorporating pre-growth had little impact on evolution dynamics (Figure S29).

At the beginning of each selection cycle, a random number was used to seed the random number generator for each Newborn community. This number was saved so that the maturation of each Newborn community can be replayed. In most simulations, the initial amount of Resource was 1 unit of $\widetilde{R}(0)$ unless otherwise specified, the initial Byproduct was $B(0) = 0$ and the initial Product $P(0) = 0$.

The maturation time T was divided into time steps of $\Delta\tau = 0.05$. Resource $R(t)$ and Byproduct $B(t)$ during each time interval $[\tau,\, \tau + \Delta\tau]$ were calculated by solving the following equations (similar to Eqs. 9-10) using the initial condition $R(\tau)$ and $B(\tau)$ via the ode23s solver in Matlab:

$$\frac{dR}{dt} = -c_{RM} g_M(R,\, B) M(\tau) - c_{RH} g_H(R) H(\tau) \tag{21}$$

$$\frac{dB}{dt} = g_H(R) H(\tau) - c_{BM} g_M(R,\, B) M(\tau) \tag{22}$$

where $M(\tau)$ and $H(\tau)$ were the biomass of M and H at time τ (treated as constants during time interval $[\tau,\, \tau+\Delta\tau]$), respectively. The solutions from Eq. 21 and 22 were used in the integrals below to calculate the biomass growth of H and M cells.

Suppose that H and M were rod-shaped organisms with a fixed diameter. Thus, the biomass of an H cell at time τ could be written as the length variable $L_H(\tau)$. The continuous growth of L_H during τ and $\tau + \Delta\tau$ could be described as

$$\frac{dL_H}{dt} = g_H(R) L_H$$

or

$$\ln \frac{L_H(\tau + \Delta\tau)}{L_H(\tau)} = \int_{\tau}^{\tau+\Delta\tau} g_H(R) dt.$$

Thus,

$$L_H(\tau + \Delta\tau) = L_H(\tau) \exp\left(\int_{\tau}^{\tau+\Delta\tau} g_H(R) dt \right). \tag{23}$$

Similarly, let the length of an M cell be $L_M(\tau)$. The continuous growth of M could be described as

$$\frac{dL_M}{dt} = (1 - f_P)g_M(R,\, B)L_M.$$

Thus for an M cell, its length $L_M(\tau + \Delta\tau)$ could be described as

$$L_M(\tau + \Delta\tau) = L_M(\tau) \exp\left(\int_{\tau}^{\tau+\Delta\tau} (1 - f_P)g_M(R,\, B)dt\right). \tag{24}$$

From Eq. 7 and 8, within $\Delta\tau$,

$$\begin{aligned}\frac{dP}{dt} &= f_P g_M(R,\, B)M \\ &\sim \frac{f_P}{1 - f_P}\frac{dM}{dt}\end{aligned}$$

and therefore

$$P(\tau + \Delta\tau) = P(\tau) + \frac{f_P}{1 - f_P}\left(M(\tau + \Delta\tau) - M(\tau)\right)$$

where $M(\tau + \Delta\tau) = \sum L_M(\tau + \Delta\tau)$ represented the sum of the biomass (or lengths) of all M cells at $\tau + \Delta\tau$.

At the end of each $\Delta\tau$, each H and M cell had a probability of $\delta_H\Delta\tau$ and $\delta_M\Delta\tau$ to die, respectively. This was simulated by assigning a random number between [0, 1] for each cell. Cells assigned with a random number less than $\delta_H\Delta\tau$ or $\delta_M\Delta\tau$ then got eliminated. For surviving cells, if a cell's length ≥ 2, this cell would divide into two cells with half the original length.

After division, each mutable phenotype of each cell had a probability of P_{mut} to be modified by a mutation (Methods, Section 4). As an example, let's consider mutations in f_P. If a mutation occurred, then f_P would be multiplied by $(1 + \Delta f_P)$, where Δf_P was determined as below.

First, a uniform random number u_1 between 0 and 1 was generated. If $u_1 \leq 0.5$, $\Delta f_P = -1$, which represented 50% chance of a null mutation ($f_P = 0$). If $0.5 < u_1 \leq 1$, Δf_P followed the distribution defined by Eq. 20 with $s_+(f_P) = 0.05$ for f_P-enhancing mutations and $s_-(f_P) = 0.067$ for f_P-diminishing mutations when epistasis was not considered (Methods, Section 4). In the simulation, Δf_P was generated via inverse transform sampling. Specifically, $C(\Delta f_P)$, the cumulative distribution function (CDF) of Δf_P , could be found by integrating Eq. 19 from -1 to Δf_P:

$$\begin{aligned}C(\Delta f_P) &= \int_{-1}^{\Delta f_P} \mu_{\Delta s}(x)dx \\ &= \begin{cases} \frac{s_-}{s_+ + s_-(1-e^{-1/s_-})}\left(\exp(\Delta f_P/s_-) - \exp(-1/s_-)\right) & \text{if } \Delta f_P \leq 0 \\ 1 - \frac{s_+}{s_+ + s_-(1-e^{-1/s_-})}\exp(-\Delta f_P/s_+) & \text{if } \Delta f_P \geq 0 \end{cases}\end{aligned} \tag{25}$$

The two parts of Eq. 25 overlap at $C(\Delta f_P = 0) = s_-(1-\exp(-1/s_-))/\left[s_+ + s_-(1 - \exp(-1/s_-))\right]$.

In order to generate Δf_P satisfying the distribution in Eq. 19, a uniform random number u_2 between 0 and 1 was generated and we set $C(\Delta f_P) = u_2$. Inverting Eq. 25 yielded

$$\Delta f_P = \begin{cases} s_- \ln\left(u_2(s_+ + s_-(1-e^{-1/s_-}))/s_- + e^{-1/s_-}\right) & u_2 \le \frac{s_-(1-e^{-1/s_-})}{s_+ + s_-(1-e^{-1/s_-})} \\ -s_+ \ln\left((1-u_2)(s_+ + s_-(1-e^{-1/s_-}))/s_+\right) & u_2 > \frac{s_-(1-e^{-1/s_-})}{s_+ + s_-(1-e^{-1/s_-})} \end{cases} \tag{26}$$

When epistasis was considered, $s_+(f_P) = s_{+init}/(1 + g \times (f_P/f_{P,init} - 1))$ and $s_-(f_P) = s_{-init} \times (1 + g \times (f_P/f_{P,init} - 1))$ were used in Eq. 26 to calculated Δf_P for each cell. (Methods Section 5).

If a mutation increased or decreased the phenotypic parameter beyond its bound (Table 1), the phenotypic parameter was set to the bound value.

The above growth/death/division/mutation cycle was repeated from time 0 to T. Note that since the size of each M and H cell can be larger than 1, the integer numbers of M and H cells, I_M and I_H, are generally smaller than the numerical values of biomass M and H, respectively. At the end of T, Adult communities were sorted according to their $P(T)$ values. The Adult community with the highest $P(T)$ (or a randomly-chosen Adult in control simulations) was selected for reproduction.

Before community reproduction, the current random number generator state was saved so that the random partitioning of Adult communities could be replayed. To mimic partitioning Adult communities via pipetting into Newborn communities with an average total biomass of BM_{target}, we first calculated the fold by which this Adult would be diluted as $n_D = \lfloor (M(T) + H(T))/BM_{target} \rfloor$. Here $BM_{target} = 100$ was the pre-set target for Newborn total biomass, and $\lfloor x \rfloor$ is the floor (round down) function that generates the largest integer that is smaller than x. If the Adult community had $I_H(T)$ H cells and $I_M(T)$ cells, $I_H(T) + I_M(T)$ random integers between 1 and n_D were uniformly generated so that each M and H cell was assigned a random integer between 1 and n_D. All cells assigned with the same random integer were then assigned to the same Newborn, generating n_D newborn communities. This partition regimen can be experimentally implemented by pipetting $1/n_D$ volume of an Adult community into a new well. If n_D was less than n_{tot} (the total number of communities under selection), all n_D newborn communities were kept and the Adult with the next highest function was partitioned to obtain an additional batch of Newborns until we obtain n_{tot} Newborns. The next cycle then began.

To fix $BM(0)$ to BM_{target} and $\phi_M(0)$ to $\phi_M(T)$ of the parent Adult, the code randomly assigned M cells from the selected Adult until the total biomass of M came closest to $BM_{target}\phi_M(T)$ without exceeding it. H cells were assigned similarly. Because each M and H cells had a length between 1 and 2, the biomass of M could vary between $BM_{target}\phi_M(T) - 2$ and $BM_{target}\phi_M(T)$ and the biomass of H could vary between $BM_{target}(1 - \phi_M(T)) - 2$ and $BM_{target}(1 - \phi_M(T))$. Variations in $BM(0)$ and $\phi_M(0)$ were sufficiently small so that community selection improved $\overline{f}_P(T)$ (Figure 5 K and L). We also simulated sorting cells so that the H and M cell numbers (instead of biomass) were fixed in Newborns. Specifically, $\lfloor BM_{target}\varphi_M(T)/1.5 \rfloor$ M cells and $\lfloor BM_{target}(1 - \varphi_M(T))/1.5 \rfloor$ H cells were sorted into each Newborn community, where we assumed that the average biomass of a cell was 1.5, and $\varphi_M(T) = I_M(T)/(I_M(T) + I_H(T))$ was calculated from cell numbers. We obtained the same conclusion (Figure S15, right panels).

To fix Newborn total biomass $BM(0)$ to the target total biomass BM_{target} while allowing $\phi_M(0)$ to fluctuate (Figure 5 D and E), H and M cells were randomly assigned to a Newborn community until $BM(0)$ came closest to BM_{target} without exceeding it (otherwise, $P(T)$ might exceed the theoretical maximum). For example, suppose that a certain number of M and H cells had been sorted into a Newborn so that the total biomass was 98.6. If the next cell, either M or H, had a biomass of 1.3, this cell would go into the community so that the total biomass would be $98.6 + 1.3 = 99.9$. However, if a cell of mass 1.6 happened to be picked, this cell would not go into this community so that this Newborn had a total biomass of 98.6 and the cell of mass 1.6 would go to the next Newborn. Thus, each Newborn might not have exactly the biomass of BM_{target}, but rather between $BM_{target} - 2$ and BM_{target}. Experimentally, total biomass can be determined from the optical density, or from the total

fluorescence if cells are fluorescently labeled ([50]). To fix the total cell number (instead of total biomass) in a Newborn, the code randomly assigned a total of $\lfloor BM_{target}/1.5 \rfloor$ cells into each Newborn, assuming an average cell biomass of 1.5. We obtained the same conclusion, as shown in Figure S15.

To fix $\phi_M(0)$ to $\phi_M(T)$ of the selected Adult community from the previous cycle while allowing $BM(0)$ to fluctuate (Figure 5 G and H), the code first calculated dilution fold n_D in the same fashion as mentioned above. If the Adult community had $I_H(T)$ H cells and $I_M(T)$ cells, $I_M(T)$ random integers between [1, n_D] were then generated for each M cell. All M cells assigned the same random integer joined the same Newborn community. The code then randomly dispensed H cells into each Newborn until the total biomass of H came closest to $M(0)(1-\phi_M(T))/\phi_M(T)$ without exceeding it, where $M(0)$ was the biomass of all M cells in this Newborn community. Again, because each M and H had a biomass (or length) between 1 and 2, $\phi_M(0)$ of each Newborn community might not be exactly $\phi_M(T)$ of the selected Adult community. We also performed simulations where the ratio between M and H cell numbers in the Newborn community, $I_M(0)/I_H(0)$, was set to $I_M(T)/I_H(T)$ of the Adult community, and obtain the same conclusion (Figure S15 center panels).

7 Problems associated with alternative definitions of community function and alternative means of reproducing an Adult

Here we describe problems associated with two alternative definitions of community function and one alternative method of community reproduction.

One alternative definition of community function is Product per M biomass in an Adult community: $P(T)/M(T)$. To illustrate problems with this definition, let's calculate $P(T)/M(T)$ assuming that cell death is negligible. From Eq. 7 and 8,

$$\frac{dM}{dt} = (1-f_P)g_M M$$

$$\frac{dP}{dt} = f_P g_M M$$

where biomass growth rate g_M is a function of B and R. Thus,

$$\frac{dM}{(1-f_P)dt} = \frac{dP}{f_P dt}$$

and we have

$$P(T) = \frac{f_P}{1-f_P}\left(M(T) - M(0)\right) \approx \frac{f_P}{1-f_P} M(T)$$

if $M(T) \gg M(0)$ (true if T is long enough for cells to double at least three or four times).

If we define community function as $P(T)/M(T) \approx \frac{f_P}{1-f_P}$, then higher community function requires higher $\frac{f_P}{1-f_P}$ or higher f_P. However, if we select for very high f_P, then M can go extinct (Figure 3).

If the community function is instead defined as $P(T)/M(0)$, then

$$\frac{P(T)}{M(0)} \approx \frac{f_P}{1-f_P}\frac{M(T)}{M(0)} = \frac{f_P}{1-f_P}\exp\left((1-f_P)\int_T g_M dt\right) \tag{27}$$

From Eq. 27, at a fixed f_P, $P(T)/M(0)$ increases as $\int_T g_M dt$ increases. $\int_T g_M dt$ increases as $\phi_M(0)$ decreases, since the larger fraction of Helper, the faster the accumulation of Byproduct and the larger $\int_T g_M dt$ (Figure S14B). As a result, when we select for higher $P(T)/M(0)$, we end up selecting communities with small $\phi_M(0)$ (Figure S2). This means that Manufactures could get lost during community reproduction, and community selection then fails.

In our community selection scheme, the average total biomass of Newborn communities was set to a constant BM_{target}. Alternatively, each Adult community can be partitioned into a constant number of Newborn communities. If Resource is not limiting, there is no competition between H and M, and $P(T)$ increases as $M(0)$ and $H(0)$ increase. Therefore, selection for higher $P(T)$ results in selection for higher Newborn total biomass (instead of higher f_p). This will continue until Resource becomes limiting, and then communities will get into the stationary phase.

8 f_P^* is smaller for M group than for H-M community

For groups or communities with a certain $\int_T g_M dt$, we can calculate f_P optimal for community function from Eq. 27 by setting

$$\frac{dP(T)}{df_p} = M(0)\frac{d}{df_p}\left[\frac{f_P}{1-f_P}\exp\left((1-f_P)\int_T g_M dt\right)\right] = 0$$

We have

$$\frac{1}{(1-f_P)^2}\exp\left((1-f_P)\int_T g_M dt\right) - \frac{f_P}{1-f_P}\int_T g_M dt \exp\left((1-f_P)\int_T g_M dt\right) = 0$$

or

$$1/\int_T g_M dt = f_P(1-f_P).$$

If $\int_T g_M dt \gg 1$, f_P is very small, then the optimal f_P for $P(T)$ is

$$f_P^* \approx \left(\int_T g_M dt\right)^{-1} \tag{28}$$

M grows faster in monoculture than in community because B is supplied in excess in monoculture while in community, H-supplied Byproduct is initially limiting. Thus, $\int_T g_M dt$ is larger in monoculture than in community. According to Eq. 28, $f_P^* = 1/\int_T g_M dt$ is smaller for monoculture than for community.

9 Stochastic fluctuations during community reproduction

The number of cells in a Newborn community is approximately $BM(0)/\overline{L}$, where $\overline{L}$ is the average biomass (or length) of M and H cells. This number fluctuates in a Poissonian fashion with a standard deviation of $\sqrt{BM_{target}/\overline{L}}$. As a result, the biomass of a Newborn communities fluctuates around BM_{target} with a standard deviation of $\sqrt{BM_{target}/\overline{L}} \times \overline{L} = \sqrt{BM_{target}\overline{L}}$.

Similarly, $M(0)$ and $H(0)$ fluctuate independently with a standard deviation of $\sqrt{\mathrm{E}[M(0)]\overline{L}} = \sqrt{BM_{target}\phi_M(T)\overline{L}}$ and $\sqrt{\mathrm{E}[H(0)]\overline{L}} = \sqrt{BM_{target}(1-\phi_M(T))\overline{L}}$, respectively, where "E" means the

expected value. Therefore, $M(0)/H(0)$ fluctuates with a variance of

$$\begin{aligned}\mathrm{Var}[M(0)/H(0)] &= \left(\frac{\mathrm{E}[M(0)]}{\mathrm{E}[H(0)]}\right)^2 \left[\frac{\mathrm{Var}[M(0)]}{(\mathrm{E}[M(0)])^2} - 2\frac{\mathrm{Cov}[M(0),\, H(0)]}{\mathrm{E}[M(0)]\mathrm{E}[H(0)]} + \frac{\mathrm{Var}[H(0)]}{(\mathrm{E}[H(0)])^2}\right] \\ &= \frac{\phi_M(T)}{(1-\phi_M(T))^3}\frac{\overline{L}}{BM_{target}}\end{aligned}$$

where "Cov" means covariance and "Var" means variance, and $\phi_M(T)$ is the fraction of M biomass in the Adult community from which Newborns are generated.

10 Mutualistic H-M community

In the mutualistic H-M community, Byproduct inhibits the growth of H. According to [95], the growth rate of *E. coli* decreases exponentially as the exogenously added acetate concentration increases. Thus, we only need to modify the growth of H by a factor of $\exp(-B/B_0)$ where B is the concentration of Byproduct and B_0 is the concentration of Byproduct at which H's growth rate is reduced by e^{-1}~0.37:

$$\frac{dH}{dt} = \exp\left(-\frac{B}{B_0}\right)\frac{g_{Hmax}R}{R+K_{HR}}H - \delta_H H$$

The larger B_0, the less inhibitory effect Byproduct has on H and when $B_0 \to +\infty$ Byproduct does not inhibit the growth of H. For simulations in Figure S22, we set $B_0 = 2K_{MB}$.

Acknowledgment

We thank the following for discussions: Lin Chao (UCSD), Maitreya Dunham (UW Seattle), Corina Tarnita (Princeton), Harmit Malik (Fred Hutch), Jeff Gore (MIT), Daniel Weissman (Emory), and Alvaro Sanchez (Yale). Some of these discussions took place at the 2017 "Systems Biology and Molecular Economy of Microbial Communities" workshop at the International Centre for Theoretical Physics, Trieste, Italy and at the 2018 "Physical Principles Governing the Organization of Microbial Communities" workshop at the Aspen Center for Physics, Colorado, USA. We thank Chichun Chen, Bill Hazelton, Samuel Hart, David Skelding, Doug Jackson, Maxine Linial, Delia Pinto-Santini, Kirill Korolev (Boston University), and Alex Sigal (K-RITH) for feedback on the manuscript. We are particularly indebted to Jim Bull (UT Austin) who generously provided sentence-by-sentence critique. This research was supported by the High Performance Computing Shared Resource of the Fred Hutch (P30 CA015704).

Figures

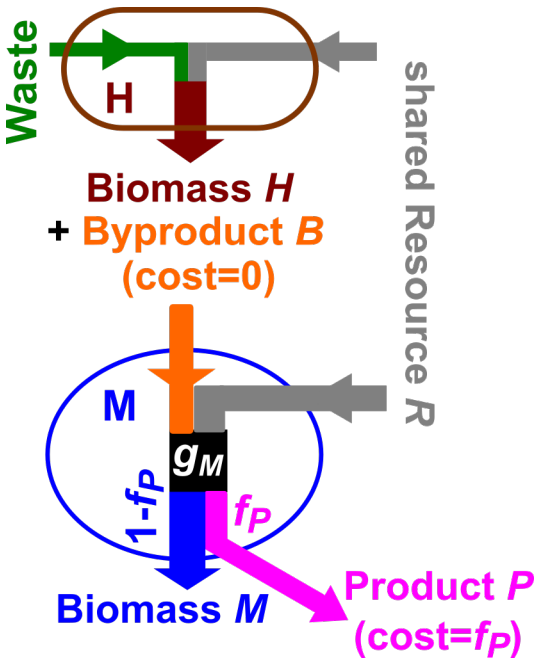

Figure 1: **A Helper-Manufacturer community that converts substrates into a product.** Helper H consumes Waste (present in excess) and Resource to grow biomass, and concomitantly releases Byproduct B at no fitness cost to itself. H's Byproduct B is required by Manufacturer M. M consumes Resource and H's Byproduct, and invests a fraction f_P of its potential growth g_M to make Product P while channeling the remaining to biomass growth. When biomass growth ceases, Byproduct and Product are no longer made. The five state variables (italicized) H, M, R, B, and P correspond to the amount of H biomass, M biomass, Resource, Byproduct, and Product in a community, respectively.

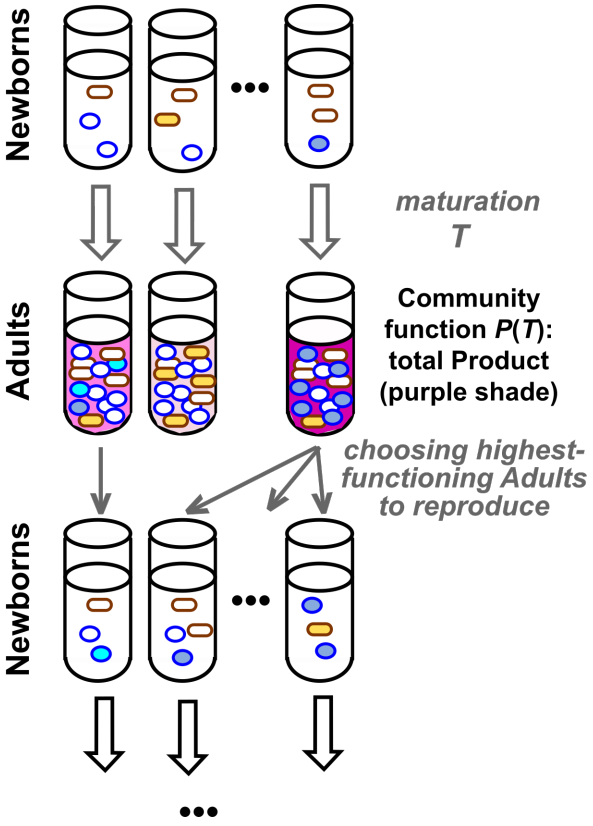

Figure 2: **Community selection scheme.** In our simulations, cycles of selection were performed on a total of $n_{tot} = 100$ communities. At the beginning of the first cycle, each Newborn had a total biomass of the target biomass (BM_{target}=100; 60 M and 40 H each of biomass 1). In subsequent cycles, species ratio would converge to the steady state value (Figure 3 bottom). Waste (not drawn) was in excess. The amount of Resource in each Newborn (not drawn) was fixed at a value that could support a total biomass of 10^4 (unless otherwise stated). The maturation time T was chosen so that for an average community, Resource was not depleted by time T (in experimental terms, this would avoid complications of the stationary phase). During maturation, Resource R, Byproduct B, Product P, and each cell's biomass were calculated from differential equations (Methods, Section 6). Once a cell's biomass had grown from 1 to 2, it divided into two identical daughter cells. Death occurred stochastically to individual cells. After division, mutations (different shades of oval and rod) occurred stochastically to change a cell's phenotypes (maximal growth rate, affinity for metabolites, and M's f_P). At the end of a cycle (time T), the top-functioning Adult with the highest Product $P(T)$ was chosen and diluted into as many Newborns as possible so that on average, each Newborn had a total biomass of approximately the target biomass BM_{target}. The next top-functioning Adult was then reproduced until $n_{tot} = 100$ Newborns were generated for the next selection cycle.

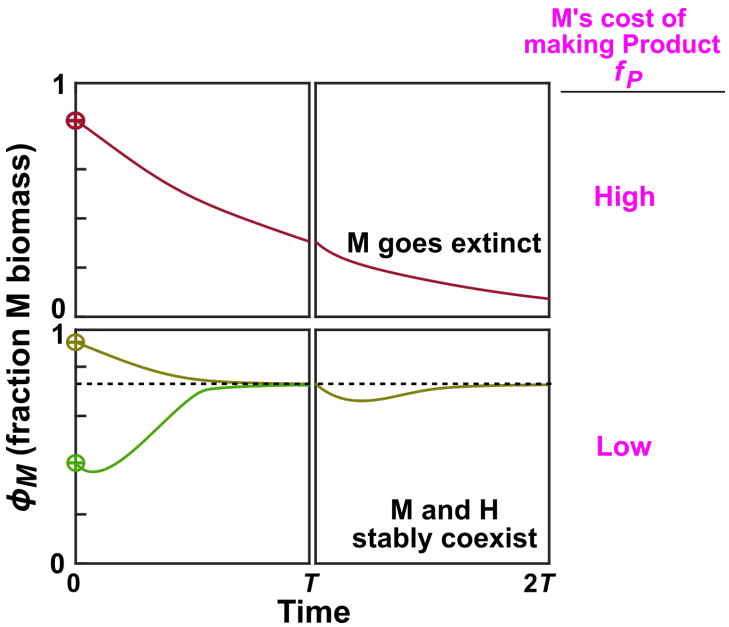

Figure 3: **H and M can stably coexist at low** f_P. Here, we plotted the fraction of M biomass in a community over two maturation cycles. **Top**: When f_P**,** the fraction of potential growth Manufacturer diverts for making Product, is high (e.g. $f_P = 0.8$), M goes extinct. **Bottom**: At low f_P (e.g. $f_P = 0.1$), H and M can stably coexist. That is, different initial species ratios will converge to a steady state value. Calculations were based on equations 6-10 with parameters in the last column of Table 1 (i.e. growth parameters at evolutionary upper bounds). At the end of the first cycle (time T=17), Byproduct and Resource were re-set to the initial conditions at time zero (0 and 10^4, respectively), and total biomass was reduced to the target value BM_{target} while the fraction of M biomass ϕ_M remained the same as that of the parent community. See main text for how values of maturation time and Resource were chosen.

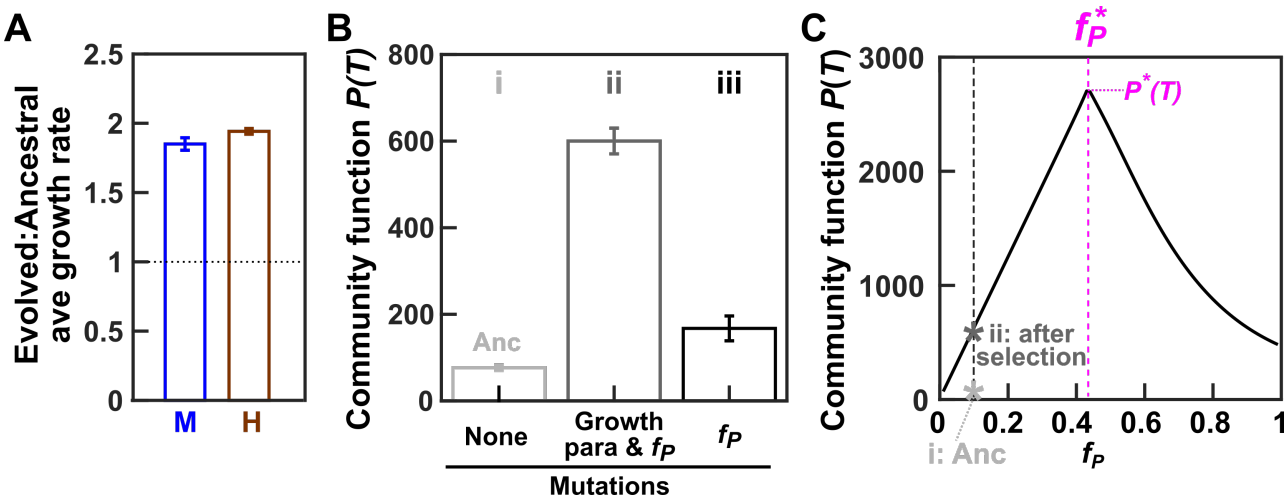

Figure 4: **Improved individual growth improved community function, although community function could be further improved.** g_{Hmax} and g_{Mmax}, H and M's maximal growth rates in excess nutrients, have evolutionary upper bounds $g^*_{Hmax}(=0.3) < g^*_{Mmax}(=0.7)$ (Table 1). (**A**-**B**) Data for selected communities from 2000th cycle are plotted, with error bars calculated form three independent selections. (**A**) The growth rates of M (blue) and H (brown) improved over ancestral values during selection. Growth rates were averaged over one selection cycle. (**B**) Community function improved largely due to mutations in growth parameters. Compared to ancestral community function where no mutations were allowed (i), community function improved when growth parameters and f_P were allowed to mutate (ii). Preventing mutations in growth parameters diminished community function improvement (iii). (**C**) Community function could be further improved. When Newborn total biomass was fixed to 100 cells and maturation time $T = 17$ time units, maximal $P(T)$ was achieved at an intermediate $f^*_P = 0.41$ (magenta dashed line), as plotted here for the species composition optimal for community function (46 H and 54 M cells in Newborn). Note that at zero f_P, no Product would be made; at high f_P, M would go extinct (Figure 3 top panel). For comparison, we plot data from B(i) (ancestral f_P and growth parameters; light grey star) and B(ii) (after community selection where f_P remained ancestral while growth parameters improved to upper bounds; dark grey star). The maximal $P^*(T)$ could not be further improved even if we allowed all growth parameters and f_P to mutate (Figure S12). Thus, $P^*(T)$ is locally maximal in the sense that small deviation will always reduce $P(T)$. Similar to other simulations, Newborns had a fixed Resource (10^4) and excess Waste.

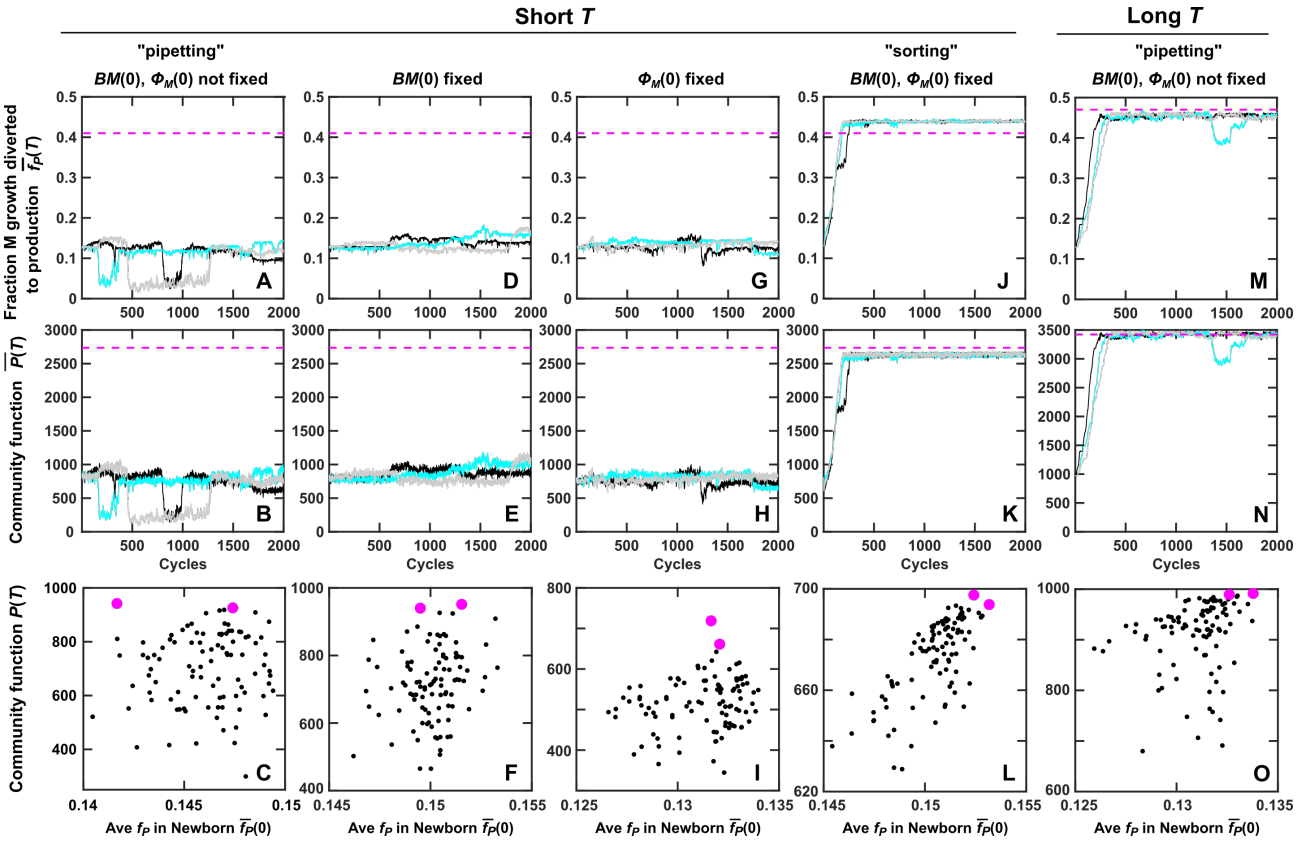

Figure 5: **Community selection succeeds when community function correlates with its heritable determinant.** (**A**-**L**) Outcome of community selection when maturation time T was sufficiently short to avoid Resource depletion and stationary phase ($T = 17$). (**A**-**C**) When the selected Adults were diluted into Newborns through pipetting (i.e. $BM(0)$ and $\phi_M(0)$ fluctuated around their respective mean values), community selection was not effective. Average f_P and community function failed to improve to their theoretical optima (magenta dashed lines), and community function poorly correlated with its heritable determinant $\overline{f}_P(0)$. Black and magenta dots: unselected and selected Adult communities from one selection cycle, respectively. (**J**-**L**) When a fixed H biomass and M biomass from the selected Adults were sorted into Newborns, community selection was successful. Community function also correlated with its heritable determinant $\overline{f}_P(0)$. Here, Newborn total biomass $BM(0)$ and fraction of M biomass $\phi_M(0)$ were respectively fixed to $BM_{target} = 100$ and $\phi_M(T)$ of the selected Adult of the previous cycle. (**D**-**I**) Fixing either $BM(0)$ or $\phi_M(0)$ did not significantly improve community selection. (**M**-**O**) When maturation time was long ($T = 20$) such that most Resource was consumed by the end of T, community selection was successful even without fixing $BM(0)$ or $\phi_M(0)$. Black, cyan and gray curves are three independent simulation trials. $\overline{P}(T)$ was averaged across the two selected Adults. $\overline{f}_P(T)$ was obtained by first averaging among M within each selected Adult and then averaging across the two selected Adults.

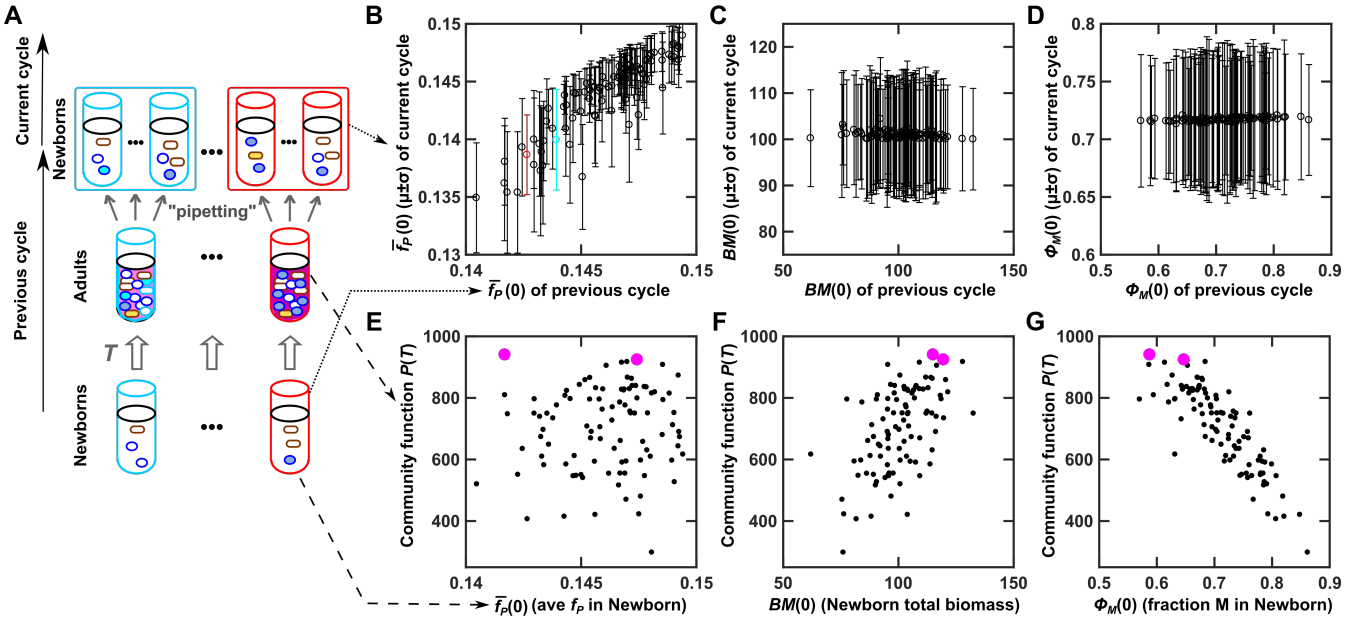

Figure 6: **During ineffective community selection, community function correlates weakly with its heritable determinant and strongly with non-heritable determinants.** (**A**) Schematic. We analyzed two consecutive cycles: In "previous cycle" (bottom), 100 Newborns matured into 100 Adults, and each Adult was then "pipetted" into multiple Newborns of the "current cycle" (top), forming 100 lineages (tubes with the same color outline belong to the same lineage). (**B**-**D**) Among the three determinants of community function, $\overline{f}_P(0)$ (f_P averaged among M cells in Newborn) is heritable, but $BM(0)$ (Newborn total biomass) and $\phi_M(0)$ (Newborn fraction of M biomass) are not. For each lineage, the community function determinant at the previous cycle was scatter plotted against those at the current cycle. For example, the abscissa of one point in **B** (e.g. red circle) indicates $\overline{f}_P(0)$ of one Newborn community from a particular lineage in the previous cycle (e.g. bottom tube of the red lineage in **A**); the ordinate and error bar of that point indicate the mean and one standard deviation of $\overline{f}_P(0)$ among the Newborn communities of that lineage from the current cycle (e.g. red box in **A**). (**E**-**G**) Correlation between each Adult community function $P(T)$ against community function determinants of the respective Newborn community. Each dot represents one community, and the two magenta dots indicate the two "successful" Newborns that achieved the highest community function at adulthood. During ineffective community selection (Figure 5B), $P(T)$ correlates weakly with heritable determinant $\overline{f}_P(0)$, but strongly with nonheritable determinants $BM(0)$ and$\phi_M(0)$.

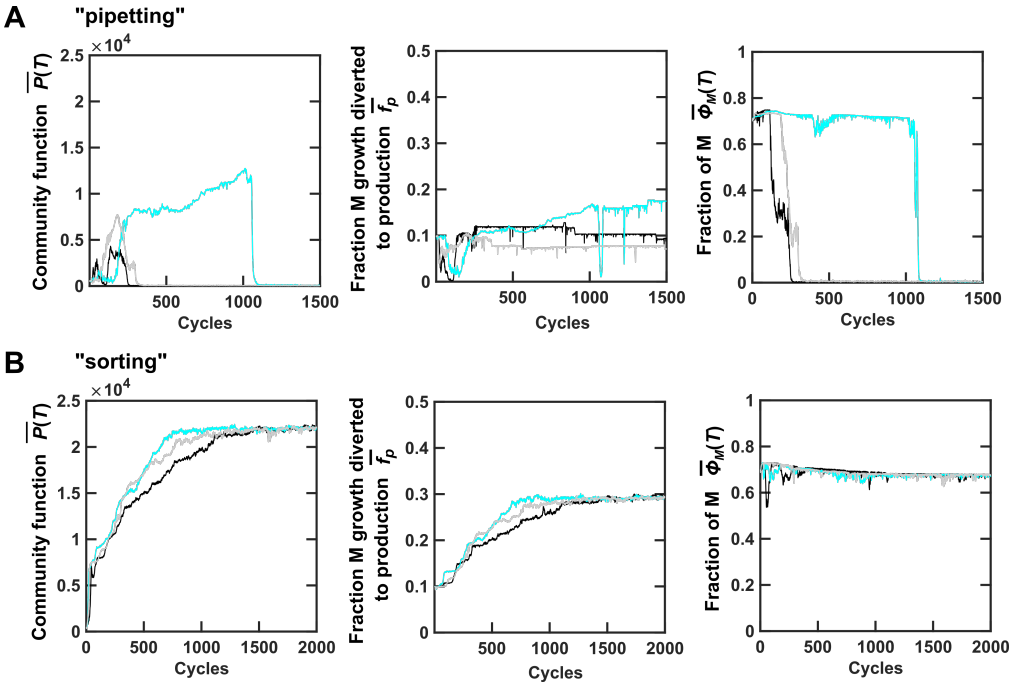

Figure 7: **Effective community selection can encourage species coexistence**. Here, the evolutionary upper bound for g_{Hmax} ($g^*_{Hmax} = 0.8$) was larger than that of g_{Mmax} ($g^*_{Mmax} = 0.7$), opposite to that in Figures 4-6. (**A**) When the selected Adult community reproduced through pipetting such that $BM(0)$ and $\phi_M(0)$ were not fixed, M was almost outcompeted by H (right) as H evolved to grow faster than M (Figure S21). Although M would ordinarily go extinct, community selection managed to maintain M at a very low level (Figure S21A, vi). This imbalanced species ratio resulted in very low community function (left). (**B**) When the selected Adult community reproduced through cell sorting such that H and M biomass were fixed in Newborns, community selection successfully improved community function and $\overline{f}_P$. Strikingly, H's growth parameters did not increase to upper bounds during effective community selection (Figure S21B), allowing a balanced species ratio (right) and high community function (left). Resource supplied to Newborn communities here supports 10^5 total biomass to accommodate faster growth rates (and hence community function is larger than in other figures). The legend is the same as in Figure 5 top and middle panels.

Supplementary Figures

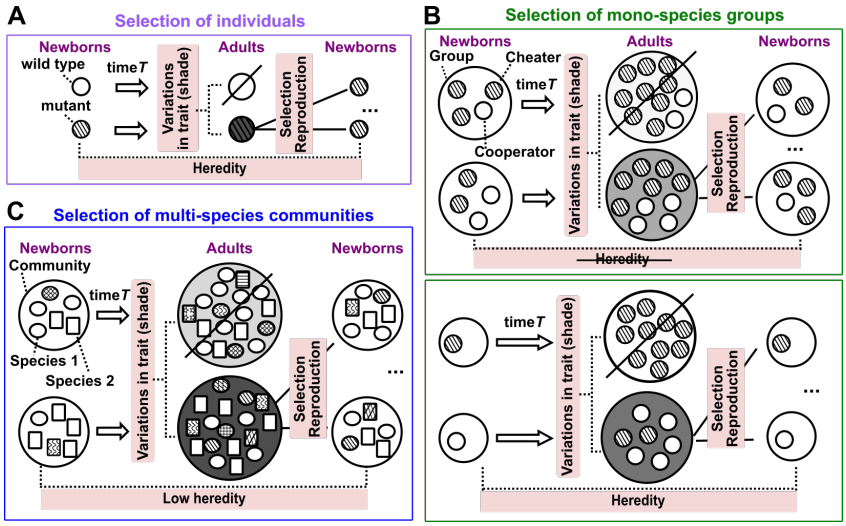

Figure S1: **Artificial selection is more challenging for multi-species communities than for individuals or mono-species groups.** Artificial selection can be applied to any population of entities [96]. An entity can be an individual (**A**), a mono-species group (**B**), or a multi-species community (**C**). Unlike natural selection which selects for fastest-growing cells, artificial selection generally selects for traits that are costly to individuals. In each selection cycle, a population of "Newborn" entities grow for maturation time T to become "Adults". Adults expressing a higher level of the trait of interest (darker shade) are selected to reproduce. An individual reproduces by making copies of itself, while an Adult group or community can reproduce by randomly splitting into multiple Newborns of the next selection cycle. Successful artificial selection requires that i) entities display trait variations; ii) trait variations can be selected to result in differential entity survival and reproduction; and iii) entity trait is sufficiently heritable from one selection cycle to the next [97]. In all three types of selection, entity variations can be introduced by mutations and recombinations in individuals. However, heredity can be low in community selection. (**A**) Artificial selection of individuals has been successful [98, 99, 100], since a trait is largely heritable so long as mutation and recombination are sufficiently rare. (**B, C**) In group and community selection, if T is small so that newly-arising genotypes cannot rise to high frequencies within a selection cycle, then Adult trait is mostly determined by Newborn *composition* (the biomass of each genotype in each member species). Then, *variation* can be defined as the dissimilarity in Newborn composition within a selection cycle, and *heredity* as the similarity of Newborn composition from one cycle to the next for Newborns connected through lineage (tubes with same-colored outlines in Figure). (**B)** Artificial selection of mono-species groups has been successful [40, 42, 13]. Suppose cooperators but not cheaters pay a fitness cost to generate a product (shade). Artificial selection for groups producing high total product favors cooperator-dominated groups, although within a group, cheaters grow faster than cooperators. At a large Newborn population size (**top**), all Newborns will harbor similar fractions of cheaters, and thus inter-group variation will be small [57]. During maturation, cheater frequency will increase, thereby diminishing heredity. In contrast, when Newborn groups are initiated at a small size such as one individual (**bottom**), a Newborn group will comprise either a cooperator or a cheater, thereby ensuring variation. Furthermore, even if cheaters were to arise during maturation, a fraction of Newborns of the next cycle will by chance inherit a cooperator, thereby ensuring some level of heredity. Thus, group selection can work when Newborn size is small. (**C**) Artificial selection of multi-species communities may be hindered by insufficient heredity. During maturation, the relative abundance of genotypes and species can rapidly change due to ecological interactions and evolution, which compromises heredity. During community reproduction, stochastic fluctuations in Newborn composition further reduce heredity.

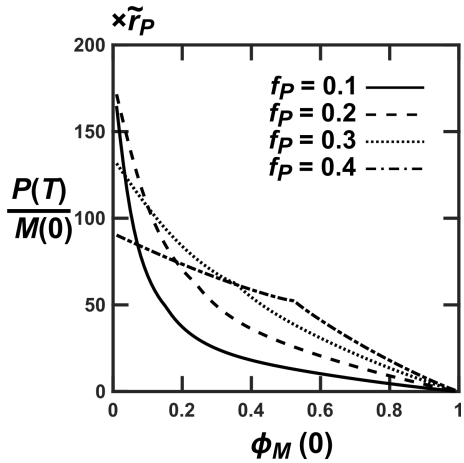

Figure S2: **Problems of defining community function as** $P(T)/M(0)$. Over the range of f_P where M and H can coexist, $P(T)/M(0)$ increases as $\phi_M(0)$ decreases. As a result, selection for higher $P(T)/M(0)$ would select communities with lower $\phi_M(0)$ and can drive M to extinction.

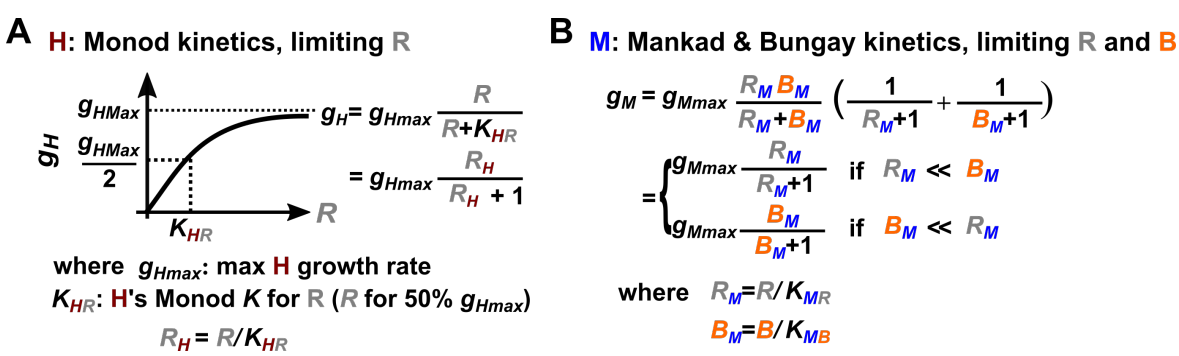

Figure S3: **Growth models of H and M.** (**A**) H growth follows Monod kinetics, reaching half maximal growth rate when $R = K_{HR}$. (**B**) M growth follows dual-substrate Mankad-Bungay kinetics. When Resource R is in great excess ($R_M \gg B_M$) or Byproduct B is in great excess ($B_M \gg R_M$), we recover mono-substrate Monod kinetics (**A**).

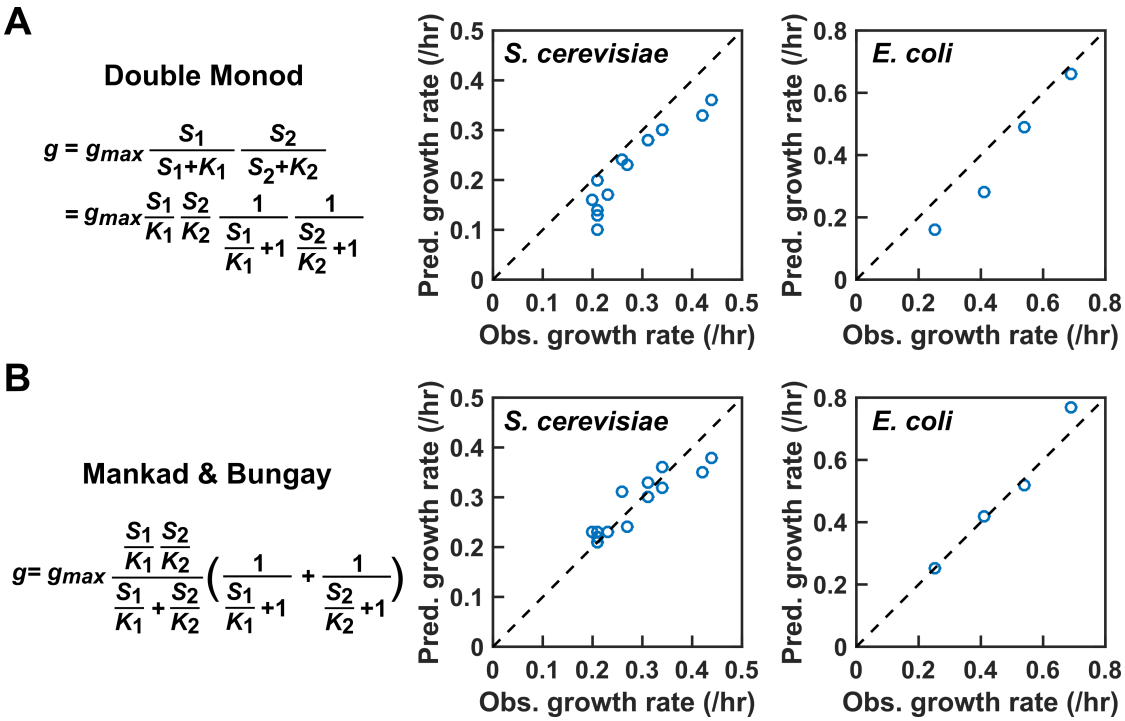

Figure S4: **A comparison of dual-substrate models.** Suppose that cell growth rate depends on each of the two substrates S_1 and S_2 in a Monod-like, saturable fashion. When S_2 is in excess, the S_1 at which half maximal growth rate is achieved is K_1. When S_1 is in excess, the S_2 at which half maximal growth rate is achieved is K_2. (**A**) In the "Double Monod" model, growth rate depends on the two limiting substrates in a multiplicative fashion. In the model proposed by Mankad and Bungay (**B**), growth rate takes a different form. In both models, when one substrate is in excess, growth rate depends on the other substrate in a Monod-fashion. However, when $\frac{S_1}{K_1} = \frac{S_2}{K_2} = 1$, the growth rate is predicted to be $g_{max}/2$ by Mankad & Bunday model, and $g_{max}/4$ by the Double Monod model. Mankad and Bungay model outperforms the Double Monod model in describing experimental data of *S. cerevisiae* and *E. coli* growing on low glucose and low nitrogen. The figures are plotted using data from Ref. [23].

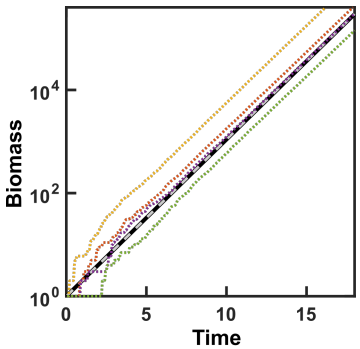

Figure S5: **A comparison of different growth models**. We model exponential biomass growth in excess metabolites. Thick black line: analytical solution with biomass growth rate (0.7/time unit). Grey dashed line: simulation assuming that biomass increases exponentially at 0.7/time unit and that cell division occurs upon reaching a biomass threshold, an assumption used in our model. Color dotted lines: simulations assuming that cell birth occurs at a probability equal to the birth rate multiplied with the length of simulation time step ($\Delta\tau = 0.05$ time unit). When a cell birth occurs, biomass increases discretely by 1, resulting in step-wise increase in color dotted lines at early time.

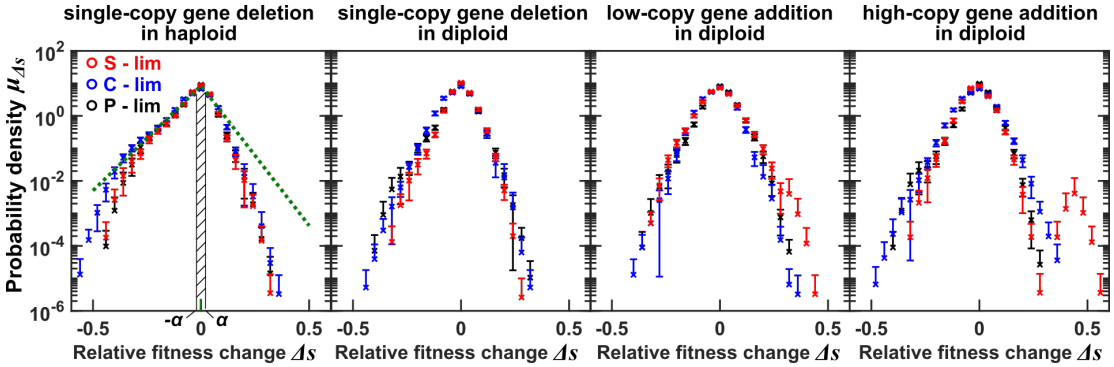

Figure S6: **Probability density functions of changes in relative fitness due to mutations (** $\mu_{\Delta s}(\Delta s)$ **).** We derived $\mu_{\Delta s}(\Delta s)$ from the Dunham lab data [32] where bar-coded mutant strains were competed under sulfate-limitation (red), carbon-limitation (blue), or phosphate-limitation (black). Error bars represent uncertainty $\delta\mu_{\Delta s}$ (the lower error bar is omitted if the lower estimate is negative). In the leftmost panel, green lines show non-linear least squared fitting of data to Eq. 19 using all three sets of data. Note that data with larger uncertainty are given less weight, and thus deviate more from the fitting. For an exponentially-distributed probability density function $p(x) = \exp(-x/r)/r$ where $x,\ r > 0$, the average of x is r. When plotted on a semi-log scale, we get a straight line with slope $1/r$, and inverting this gets us the average effect r. From the green line on the right side, we obtain the average effect of enhancing mutations $s_+ = 0.050 \pm 0.002$, and from the green line on the left side, we obtain the average effect of diminishing mutations $s_- = 0.067 \pm 0.003$. The probability of a mutation altering a phenotype by $\pm\alpha$ is the shaded area.

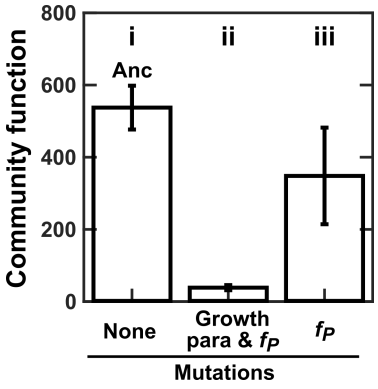

Figure S7: **Improving individual growth can impair community function.** Here, the evolutionary upper bound for g_{Hmax} ($g^*_{Hmax} = 0.8$) was larger than that of g_{Mmax} ($g^*_{Mmax} = 0.7$), opposite to that in Figure 4. If community reproduction occurred through volumetric dilution via pipetting, and if f_P and growth parameters were allowed to mutate, community function declined to below the ancestral level (left). For detailed dynamics, see Figure S21. Resource supplied to Newborn communities could support 10^5 total biomass to accommodate faster growth rate.

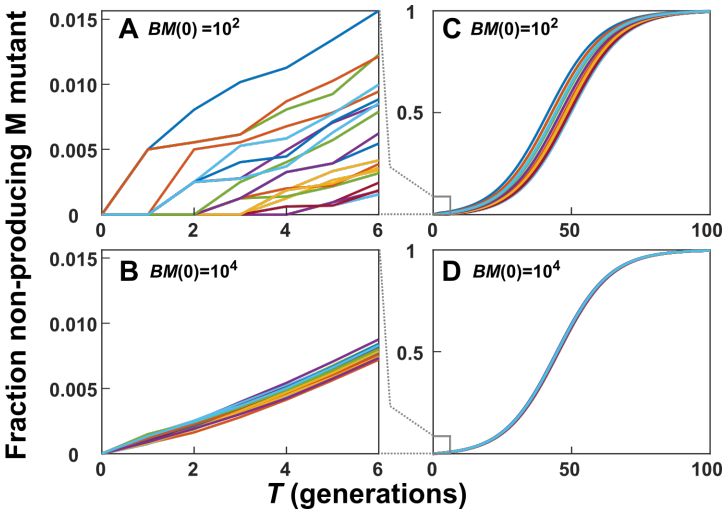

Figure S8: **Large Newborn group size or long maturation time allows non-producers to accumulate and reduces inter-group variation.** For simplicity, we modeled the growth of Newborn groups of M cells. From a Newborn biomass of 10^2 or 10^4 wild-type M cells, M population multiplied for 6 or 100 generations. Immediately following cell division, wild-type daughter cells mutated to non-producers with a probability of 10^{-3}. Wild-type and mutant cells followed exponential growth.The growth rate of wild-type cells was 0.87 times that of mutants. The fraction of biomass made up by mutants at each wild-type doubling is shown. Note the different scales.

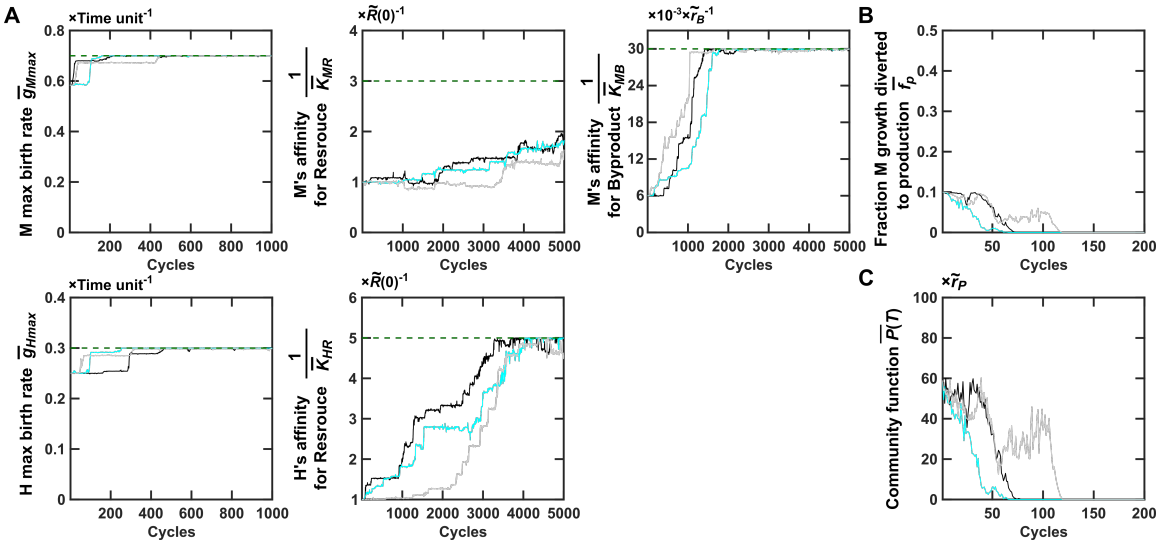

Figure S9: **Community function declines to zero in the absence of artificial selection for higher community function**. When random Adults were selected to reproduce, natural selection favored fast growers with improved maximal growth rates and improved affinities for nutrients (**A**), and zero f_P (**B**). Consequently, $P(T)$ decreased to zero (**C**). Maximal growth rates of H and M (g_{Hmax} and g_{Mmax}), H's affinity for Resource $1/K_{HR}$, and M's affinity for Byproduct $1/K_{MB}$ rapidly improved to their respective upper bounds, while M's affinity for Resource $1/K_{MR}$ improved more slowly. This is consistent with M's growth being more limited by Byproduct. Green dashed lines: upper bounds of phenotypes; Magenta dashed lines: f_P optimal for community function and maximal $P(T)$ when all five growth parameters are fixed at their upper bounds and $\phi_M(0)$ is also optimal for $P(T)$. Black, cyan, and gray curves show three independent simulations. $\overline{P}(T)$ is averaged across selected Adults. $\bar{g}_{Mmax}$, $\bar{g}_{Hmax}$, and $\overline{f}_P$ are obtained by averaging within each selected Adult and then averaging across selected Adults. $K_{SpeciesMetabolite}$ are averaged within each selected Adult, then averaged across selected Adults, and finally inverted to represent average affinity. Note different x axis scales. The maximal growth rates (g_{Mmax} and g_{Hmax}) have the unit of 1/time. Affinity for Resource ($1/K_{MR}$, $1/K_{HR}$) has the unit of $1/\widetilde{R}(0)$, where $\widetilde{R}(0)$ is the initial amount of Resource in Newborn. Affinity for Byproduct ($1/K_{MB}$) has the unit of $1/\widetilde{r}_B$, where $\widetilde{r}_B$ is the amount of Byproduct released per H biomass produced. Product P has the unit of $\widetilde{r}_P$, the amount of Product released at the cost of one M biomass. More details can be found in Table 1.

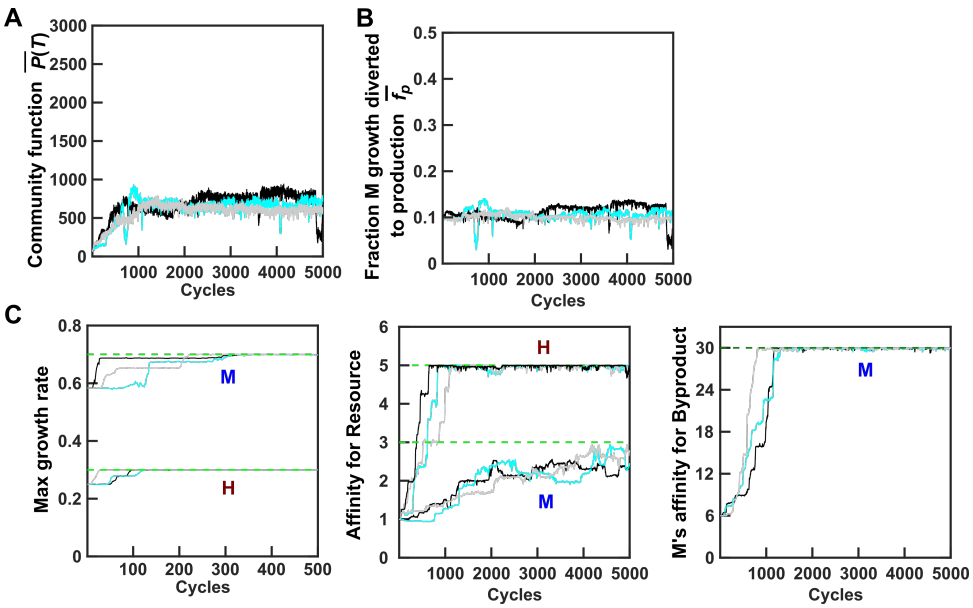

Figure S10: **Improved individual growth can promote community function.** Community function $P(T)$ increased upon community selection (**A**). Since f_P remained unchanged (**B**), this increase in $P(T)$ must be due to improved growth parameters (**C**). Other legends are the same as Figure S9.

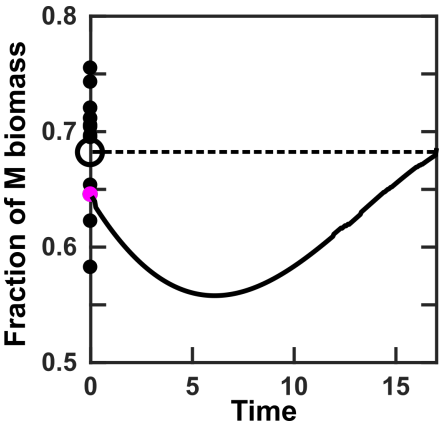

Figure S11: **The average growth rate of M exceeds the average growth rate of H in selected communities.** The fraction of M's biomass in 10 Newborns were plotted by filled dots at Time 0. Since these Newborn communities were generated via volumetric dilutions by pipetting, these fractions fluctuated stochastically around that of the parent Adult community (open black circle). Since Newborns with lower fraction of M tend to achieve higher community function (Figure 6), here the Newborn marked by the magenta dot would achieve the highest community function and thus be chosen to reproduce. In addition, its fraction of M biomass approached a steady-state value (black dashed line) upon maturation. Since the fraction of M increased from below-steady-state to steady-state, the average growth rate of M was higher than that of H. Data here are from Cycle 100 of the simulation plotted in Figure 4 i).

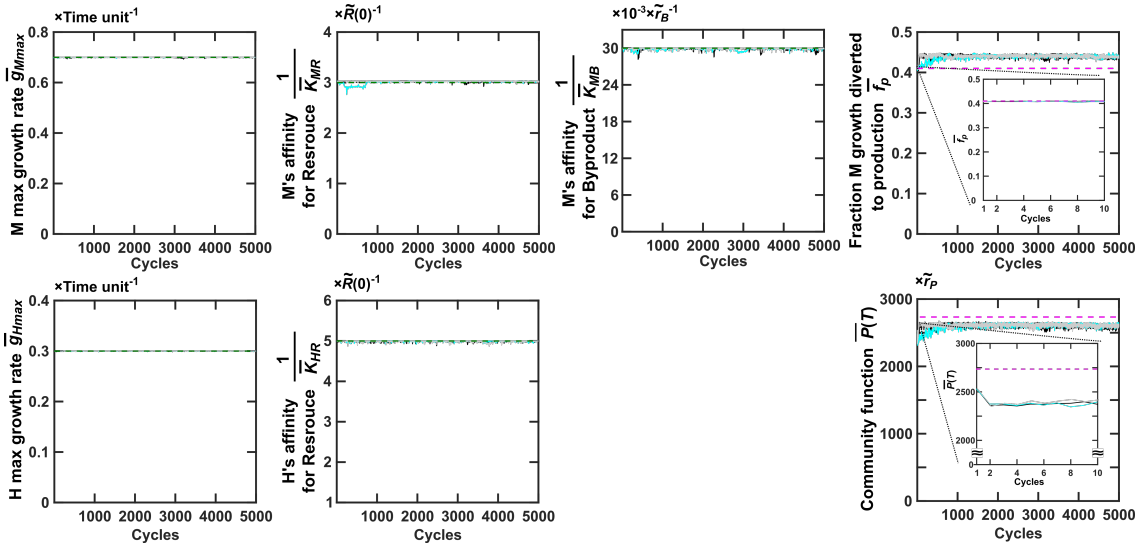

Figure S12: $P^*(T)$ **is a local optimum because it cannot be further improved.** We started each Newborn community with total biomass $BM(0) = 0$, all five growth parameters at their upper bounds, and $f_P^* = 0.41$ and $\phi_M^*(0) = 0.54$ to achieve $P^*(T)$. We then allowed all five growth parameters and f_P to mutate while applying community selection. To ensure effective community selection (Figure 5), $BM(0)$ was fixed to 100, and $\phi_M(0)$ was fixed to $\phi_M(T)$ of the selected Adult community from the previous cycle during community reproduction. We found that all five growth parameters remained at their respective evolutionary upper bounds. At the end of the first cycle (Cycle = 1 in insets), even though $\overline{f}_P$ did not change, $\overline{P}(T)$ had already declined from the original magenta dashed line. This is because species interactions have driven $\phi_M(0)$ from the optimal $\phi_M^*(0)$ $(= 0.54)$ to near the steady state value ($\phi_M = 0.72$, compare with $\phi_{M,SS}$ represented by the green dashed line in Figure 1C bottom panel). Later, over hundreds of cycles, $\overline{f}_P$ gradually increased, which increased $\overline{P}(T)$. However, $\overline{P}(T)$ was still below maximal. This is because species composition gravitated toward steady state $\phi_{M,SS}$ which deviated from the optimal $\phi_M^*(0)$ ([60]). Other legend details can be found in Figure S9.

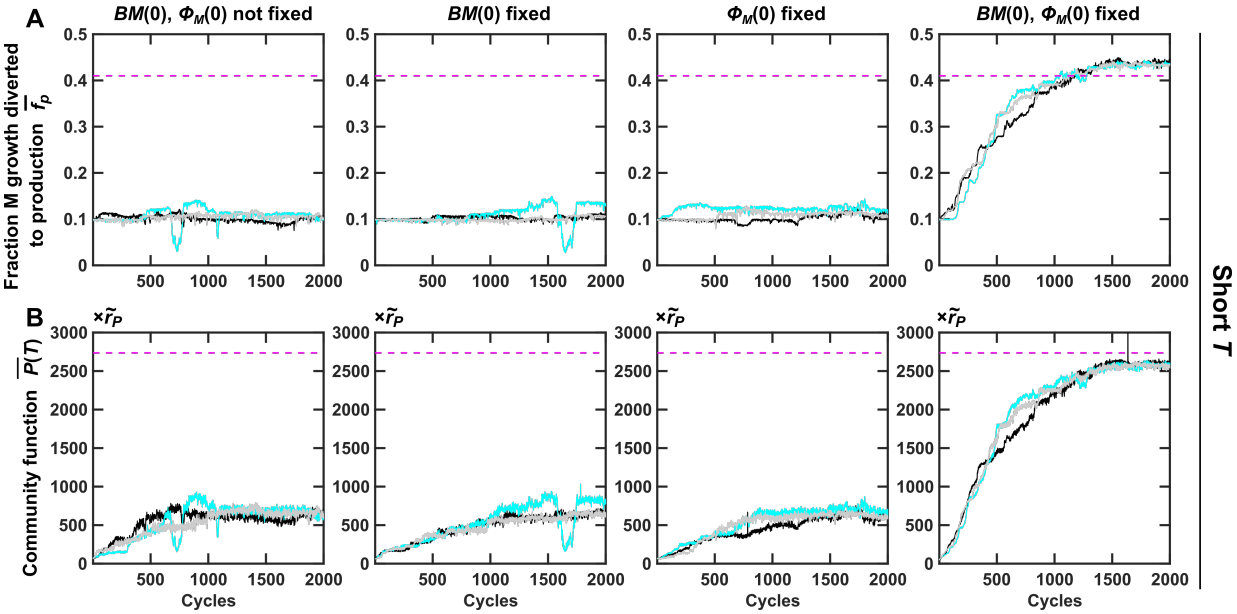

Figure S13: **Community selection succeeded under the appropriate selection regimen even if growth parameters were also allowed to be modified by mutations.** (**A**) $\overline{f}_P(T)$ and (**B**) $\overline{P}(T)$ of selected communities over 2000 selection cycles when the maturation time $T = 17$, $g^*_{Hmax} = 0.3$ and $g^*_{Mmax} = 0.7$. All other simulation parameters are in Table 1. Compared to simulations whose results are presented in Figure 5, simulations for this figure allowed growth parameters of each M and H cells, and f_P of each M cell, to vary. The legends are the same as Figure 5.

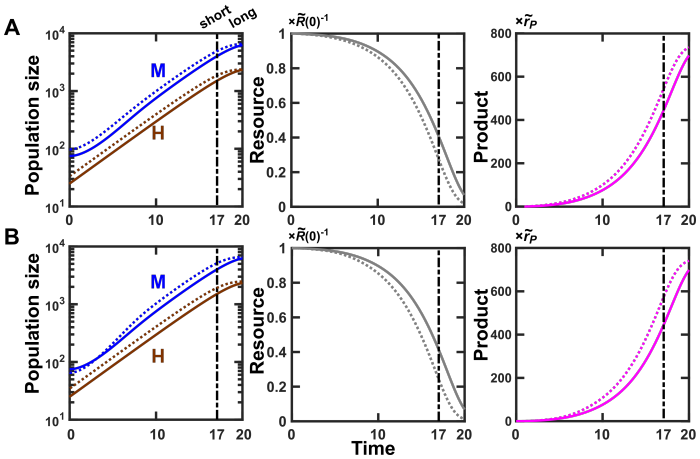

Figure S14: **Variations in community function can arise from non-heritable variations in Newborn compositions.** An average Newborn community (solid lines) has a total biomass of 100 with 75% M. (**A**) A "lucky" Newborn community (dotted lines), by stochastic fluctuations, has a total biomass of 130 with 75% M. Even though the two communities share identical $f_P = 0.1$, biomass of M in the Newborn starting with a total biomass of 130 can grow to a higher value (left), deplete more Resource (middle), and make more Product (right) by the end of short T ($T = 17$). (**B**) A "lucky" Newborn community (dotted lines), by stochastic fluctuations, has a total biomass of 100 with 65% M. Even though the two communities share identical $f_P = 0.1$, higher fraction of H biomass results in faster accumulation of Byproduct. Consequently, M cells in the Newborn with lower $\phi_M(0)$ (dotted) suffer from a shorter growth lag and can grow to a larger size (left), deplete more Resource (middle), and make more Product (right) by the end of short T ($T = 17$). In both cases, the difference between lucky (dotted) and average (solid) communities is diminished at longer T ($T = 20$) compared to shorter T ($T = 17$, dash dot line).

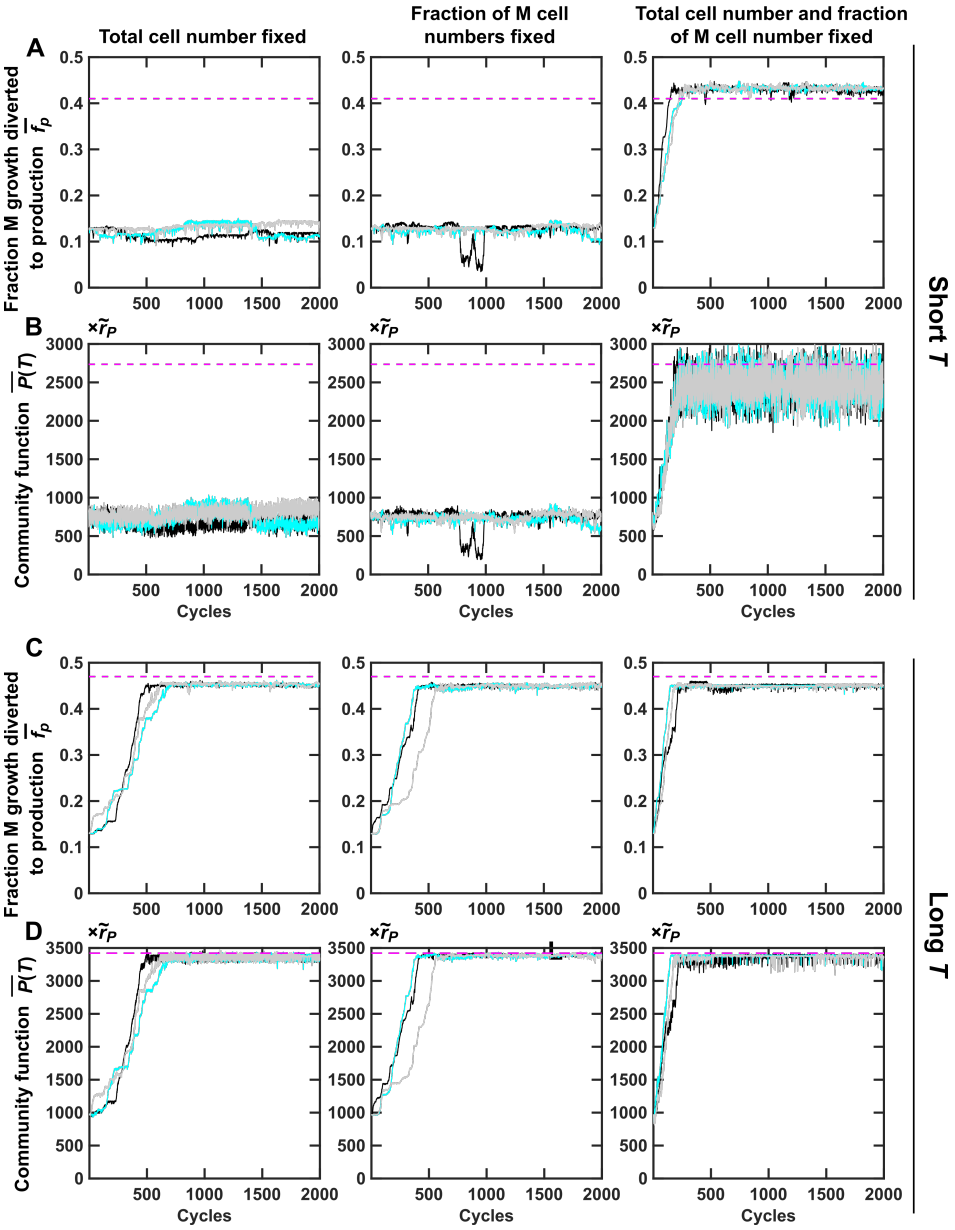

Figure S15: **Fixing H and M cell numbers (instead of biomass) during community reproduction allows short-T selection regimen to improve community function.** For left panels, the total cell number in Newborn communities was fixed to $\lfloor BM_{target}/1.5 \rfloor$ where $\lfloor x \rfloor$ means rounding down x to the nearest integer. For center panels, the ratio between M and H cell numbers in Newborn communities were fixed to $I_M(T)/I_H(T)$, where $I_M(T)$ and $I_H(T)$ were the number of M and H cells in the selected Adult community from the previous cycle, respectively. For right panels, the total cell numbers of Newborn communities were fixed to $\lfloor BM_{target}/1.5 \rfloor$ and the ratio between M and H cell numbers were fixed to $I_M(T)/I_H(T)$. See Methods Section 6 for details of simulating community reproduction. Other legend details can be found in Figure 5.

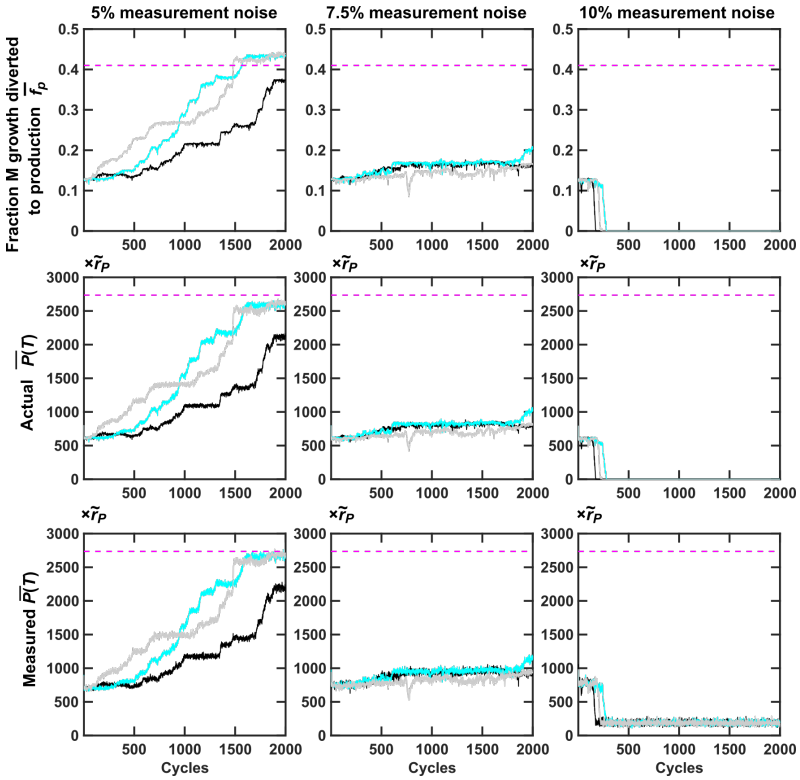

Figure S16: **High measurement uncertainty in $P(T)$ impedes community selection.** Dynamics of $\overline{f}_P(T)$ and $\overline{P}(T)$ of selected Adult communities when Adult communities were chosen to reproduce based on "measured $P(T)$" - the sum of actual $P(T)$ and an "uncertainty term" randomly drawn from a normal distribution with zero mean. In the left, center, and right panels, the uncertainty term was drawn from normal distributions with standard deviations of 5%, 7.5%, and 10% of the ancestral $P(T)$, respectively. The middle and lower panels show the average actual $P(T)$ and the average measured $P(T)$, respectively.

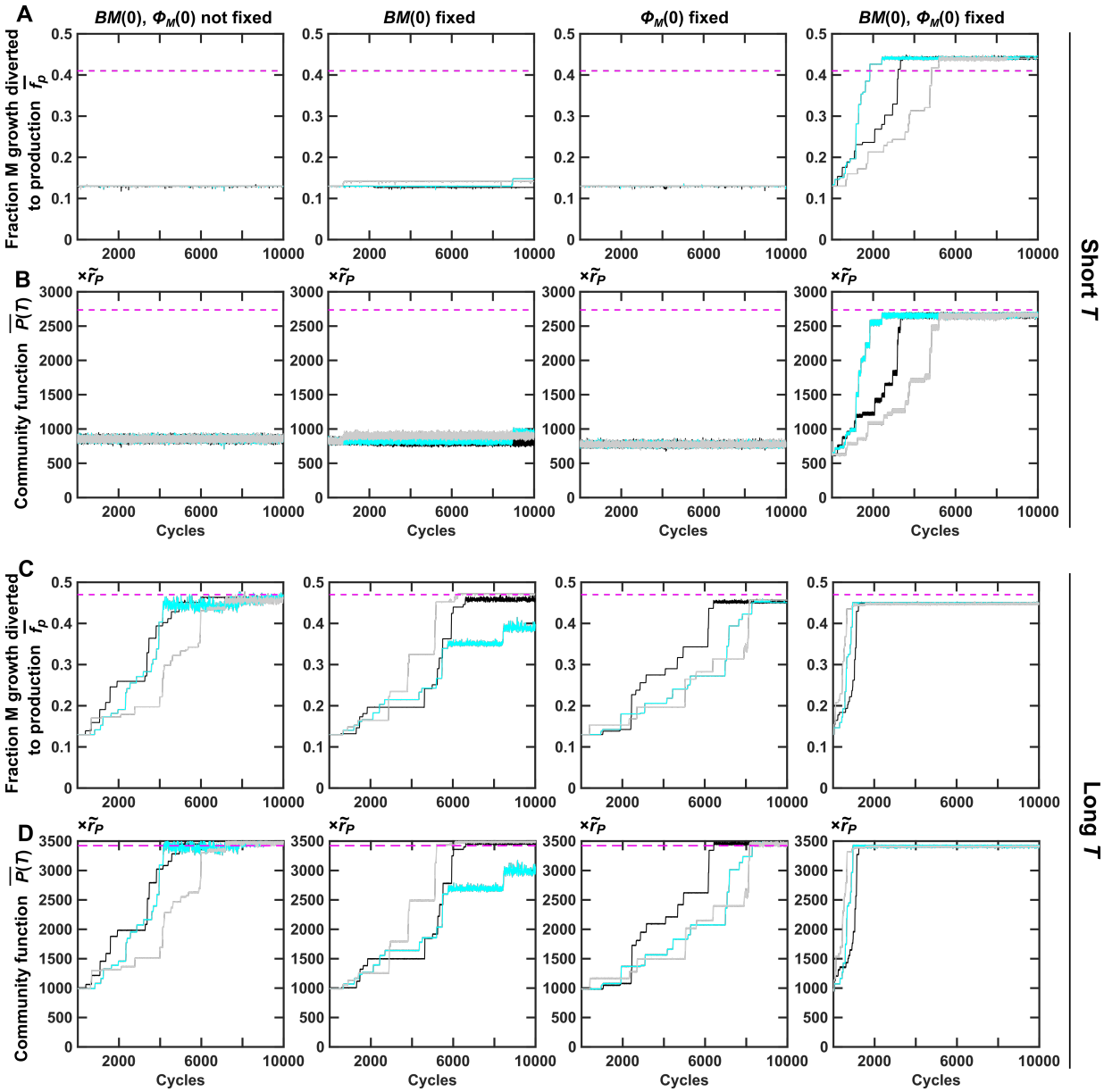

Figure S17: **Evolution dynamics of selected Adult communities at a mutation rate of 2×10^{-5} per cell per generation.** (**A, B**) At short maturation time ($T = 17$, Resource was not exhausted in an average community), fixing both $BM(0)$ and $\phi_M(0)$ was required for community function to improve. (**C, D**) At long maturation time ($T = 20$, Resource was nearly exhausted in an average community), community function improved without needing to fix $BM(0)$ or $\phi_M(0)$. When both are fixed, community function improved even faster. At this mutation rate, because the population size of a community never exceeds 10^4, a mutation occurs on average every 5 cycles, resulting in step-wise improvement in both $\overline{f}_P(T)$ and $\overline{P}(T)$. Other legend details can be found in Figure 5.

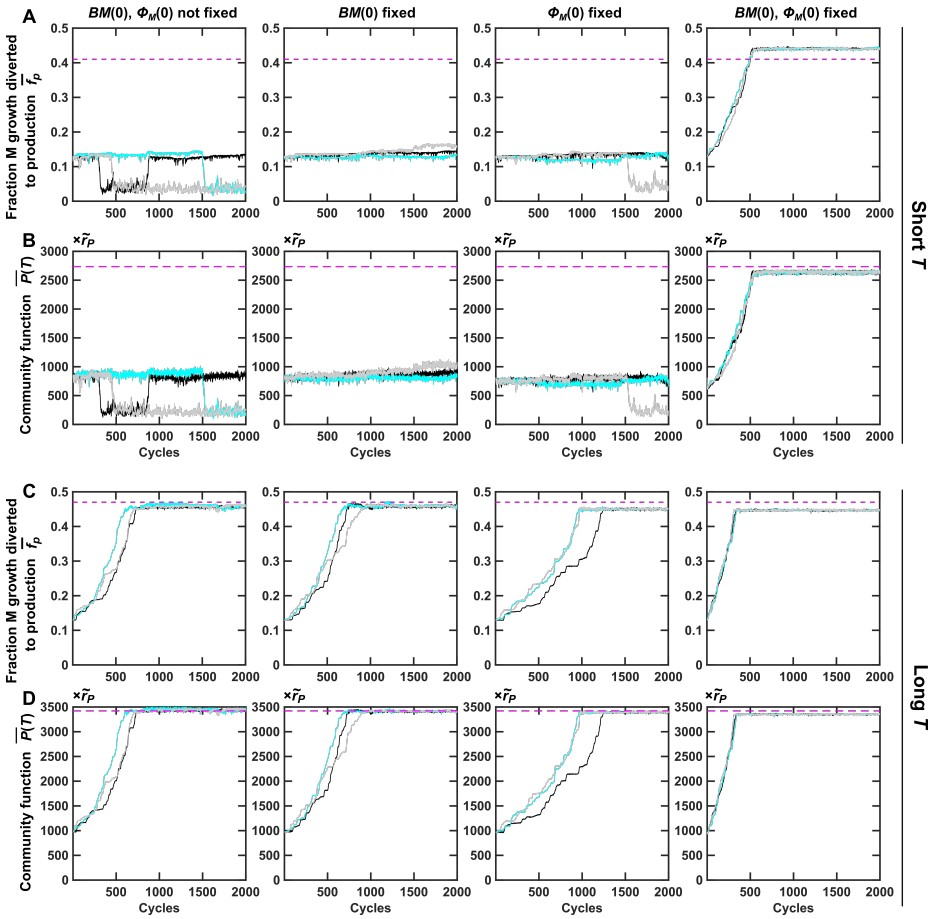

Figure S18: **Evolutionary dynamics of selected Adult communities under a different distribution of mutation effects.** Here, the distribution of mutation effects is specified by Eq. 19 where $s_+ = s_- = 0.02$ are constants. Other legend details can be found in Figure 5.

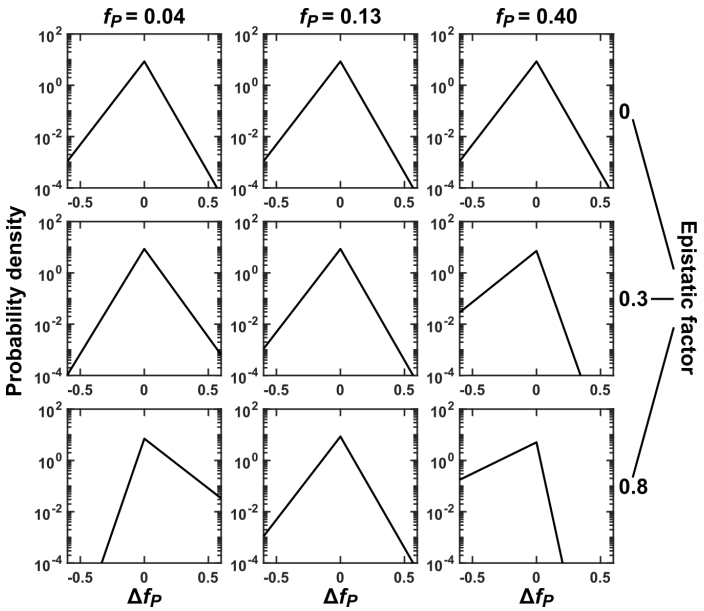

Figure S19: **Mutation effects under epistasis.** Distribution of mutation effects at different current f_P values (marked on top) are plotted. (Top) When there is no epistasis, distribution of mutational effects on f_P ($\triangle f_P$) are identical regardless of current f_P. (Middle and Bottom) With epistasis (see Methods Section 5 for definition of epistasis factor), mutational effects on f_P depend on the current value of f_P. If current f_P is low (left), enhancing mutations are more likely to occur (the area to the right of $\triangle f_P = 0$ becomes bigger) and their mean mutational effect becomes larger (mean=1/slope becomes larger due to smaller slope), while diminishing mutations are less likely to occur and their mean mutational effect is smaller. If current f_P is high (right), the opposite is true.

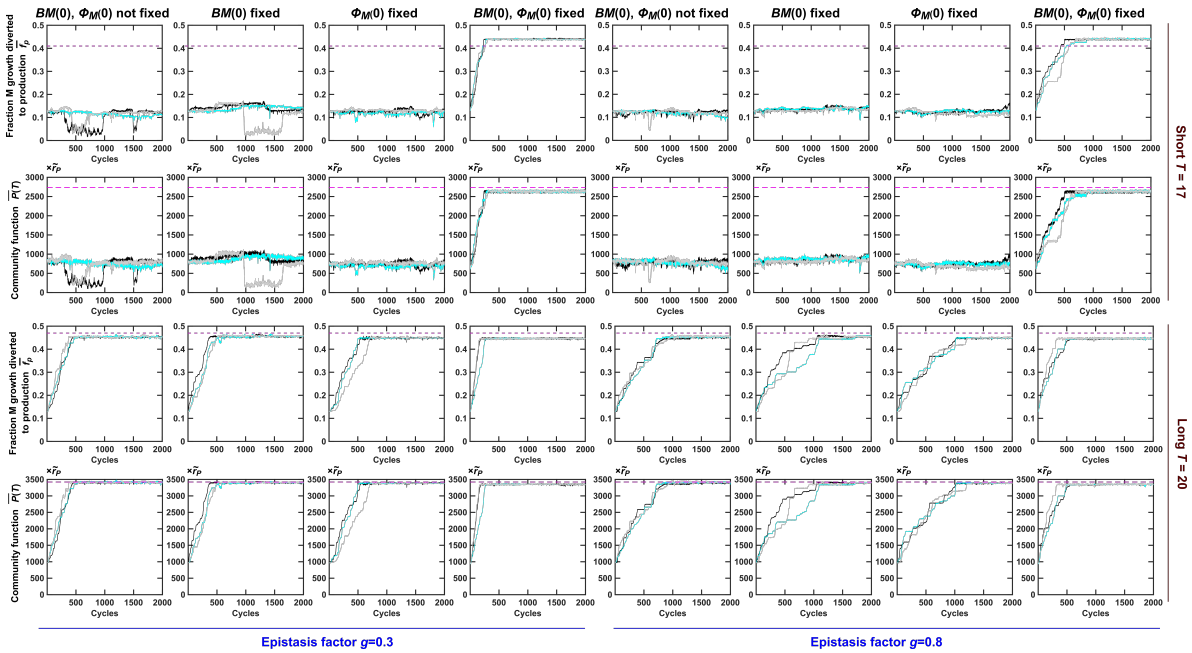

Figure S20: **Evolutionary dynamics of selected Adults when epistasis is considered.** When we incorporated different epistasis strengths (epistasis factor of 0.3 and 0.8), we obtained essentially the same conclusions as when epistasis was not considered (Figure 5). Other legend details can be found in Figure 5.

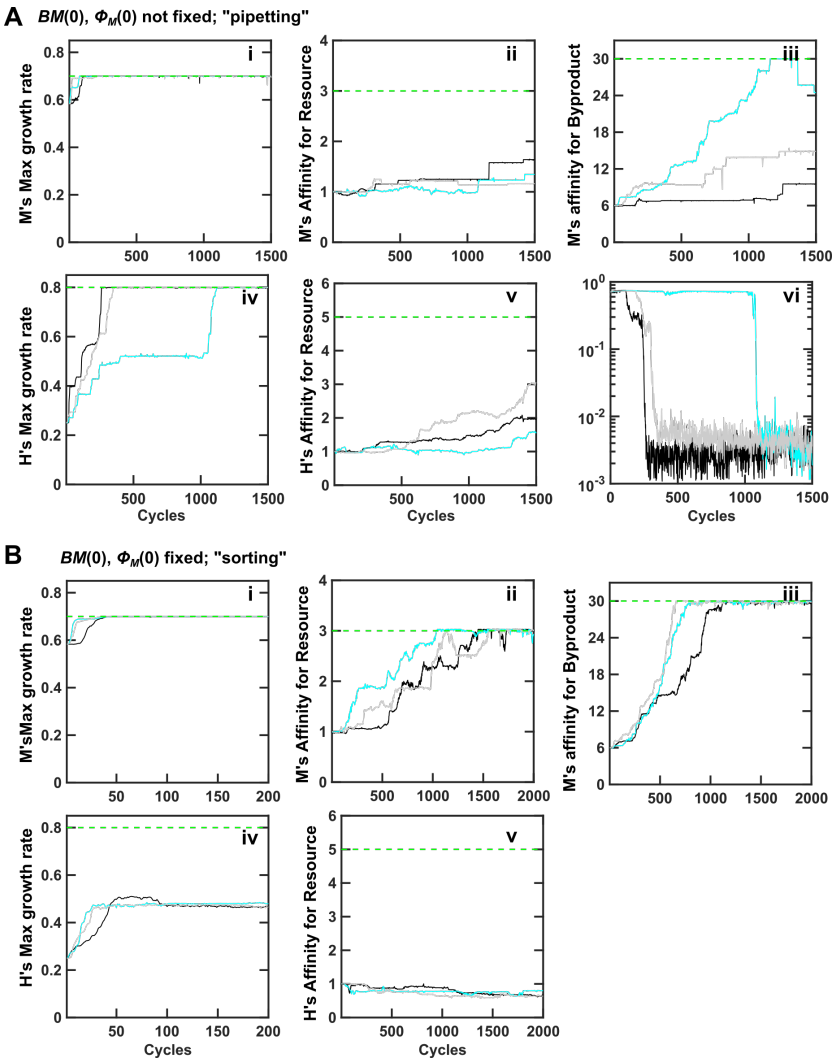

Figure S21: **Community function can be improved even if it is costly to both species.** Identical to Figures S7 and 7, the evolutionary upper bound for g_{Hmax} ($g^*_{Hmax} = 0.8$) was larger than that of g_{Mmax} ($g^*_{Mmax} = 0.7$), opposite to that in Figure 4. (**A**) Selected Adult communities were reproduced through through pipetting such that both $BM(0)$ and $\phi_M(0)$ could stochastically fluctuate. Eventually, g_{Hmax} and g_{Mmax} evolved to their respective upper bounds, and thus $g_{Hmax} > g_{Mmax}$ (compare **i** and **iv**). This would ordinarily lead to extinction of M. However, community selection managed to maintain M at a very low level (**vi**). (**B**) Selected Adult communities were reproduced through biomass sorting so that both $BM(0)$ and $\phi_M(0)$ were fixed. Community selection worked in the sense that both $\overline{f}_P$ and $P(T)$ improved over cycles (Figure 7). Strikingly, g_{Hmax} did not increase to its upper bound $g^*_{Hmax} = 0.8$, and H's affinity for Resource even decreased from the ancestral level. Here, Resource supplied to Newborn communities could support 10^5 total biomass to accommodate faster growth rate. $\overline{\phi}_M(T)$ (fraction of M biomass in Adult communities) were obtained by averaging across selected Adults. Other legend details can be found in Figure S9.

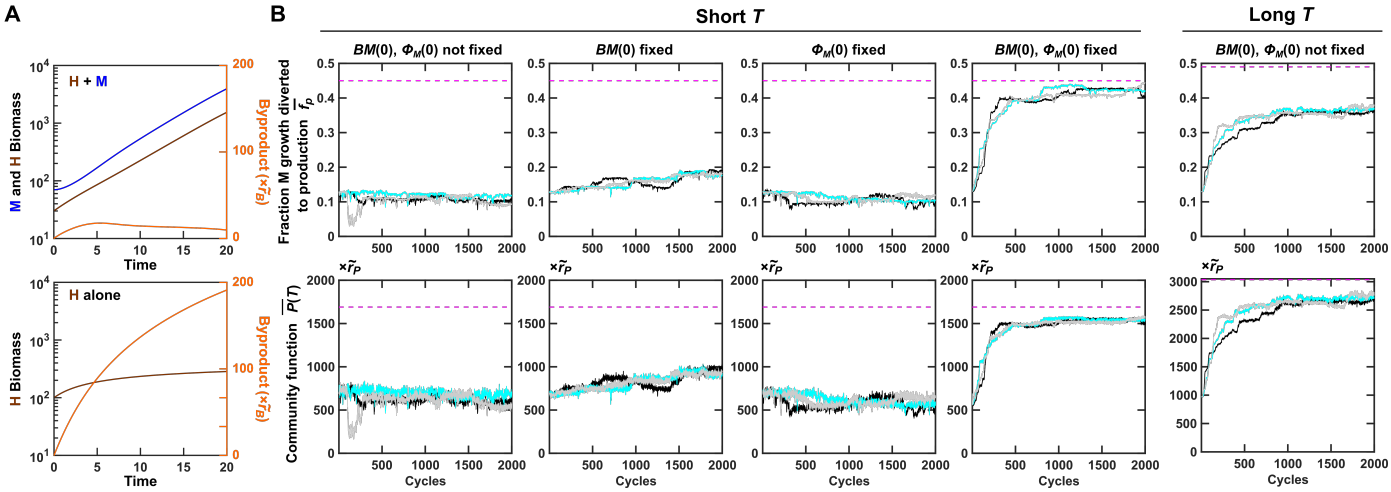

Figure S22: **Selection dynamics of mutualistic H-M communities.** In the mutualistic H-M community, H generates Byproduct which is essential for M but inhibitory to H. (**A**) H can grow to a high density in the presence of M (top) but not in the absence of M (bottom). (**B**) Similar to community selection on commensal H-M communities, selection worked when non-heritable variations in $P(T)$ were suppressed either via fixing both $BM(0)$ and $\phi_M(0)$ at short T ($T = 17$) or via extending T ($T = 20$). Other legend details can be found in Figure 5.

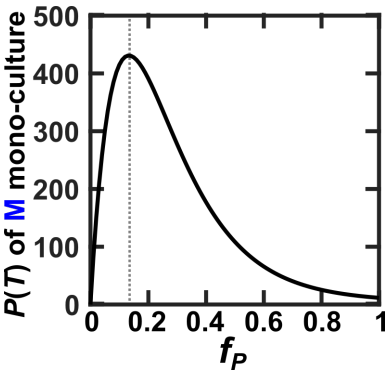

Figure S23: **Optimal f_P for accumulation of Product in an M monoculture is lower than that for an H-M community**. Suppose that a Newborn M group starts with a single Manufacturer (biomass 1) supplied with excess Byproduct and the same amount of Resource as in a Newborn H-M community. Then, maximal group function is achieved at $f_P = f^*_{P,Mono} = 0.13$ ("mono-adapted", dashed line), lower than the optimal f_P for the community function $f^*_P = 0.41$ (Figure **??**). Here, the growth parameters of M and H are all fixed at their upper bounds and $P(T)$ has the unit of $\tilde{r}_P$.

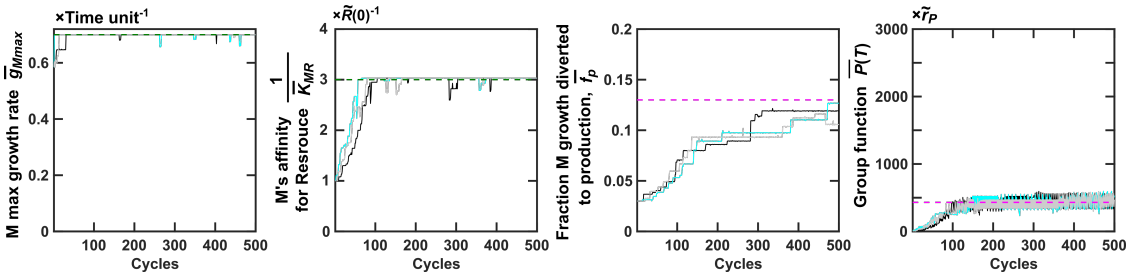

Figure S24: **Selection dynamics of M mono-species groups**. Phenotypes averaged over selected groups are plotted for 500 selection cycles. Because Byproduct is in excess, K_{MB} terms are no longer relevant in equations (Figure S4, $R_M \ll B_M$). Upper bounds of g_{Mmax} and $1/K_{MR}$ are marked with green dashed lines. Magenta lines mark f_P optimal for community function and maximal $P(T)$ when g_{Mmax} and $1/K_{MR}$ are fixed at their upper bounds and when Byproduct is in excess.

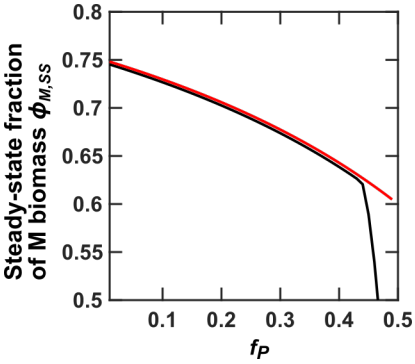

Figure S25: Comparison between the steady-state $\phi_{M,SS}$ calculated from Eqs. 6-10 (black curve) and from Eq. 14 (red line).

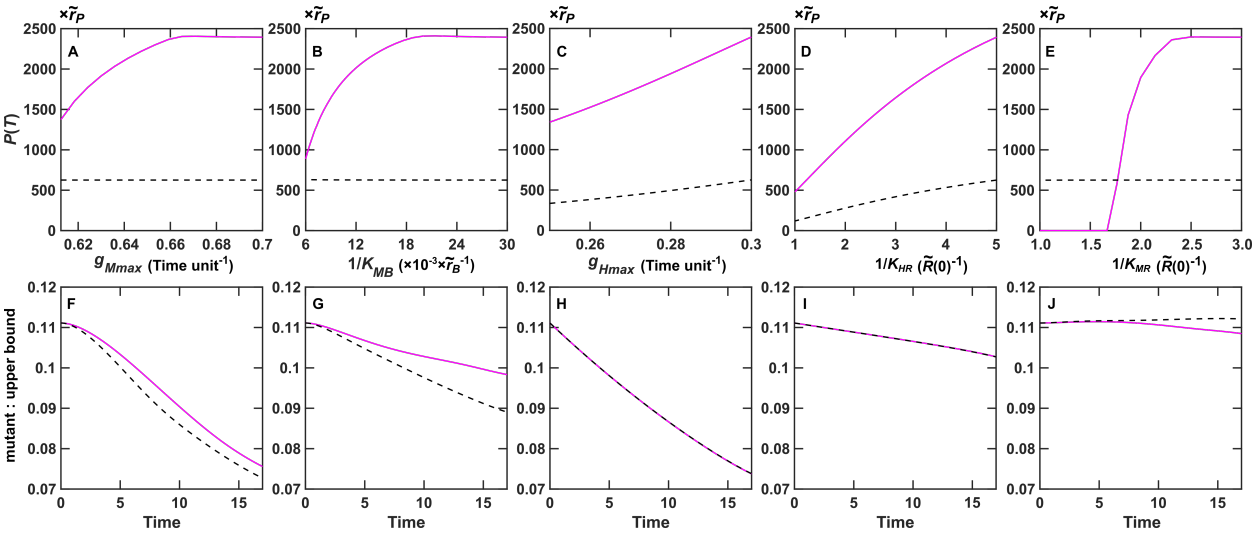

Figure S26: **Improved maximal growth rates and nutrient affinities generally, but do not always, improve individual fitness and community function.** In all figures, solid and dashed lines respectively represent calculations with $f_P = f_P^* = 0.41$ (optimal for community function; Figure **??**) and $f_P = f_{P,Mono}^* = 0.13$ (optimal for M monoculture production when Byproduct is in excess; Figure S23). Except for the indicated growth parameter, all other growth parameters were set to their respective upper bounds. (**A**-**D**) Community function increases as the indicated growth parameter increases. For example in (**A**), all growth parameters except for g_{Mmax} were set to their upper bounds. For each g_{Mmax}, the steady-state $\phi_{M,SS}$ was calculated using equations in Methods Section 1. This steady-state $\phi_{M,SS}$ was then used to calculate $P(T)$. (**F**-**I**) The ratio between mutant population (whose indicated growth parameter was 10% lower than the upper bound) and growth-adapted population over maturation time $T = 17$. The decreasing ratio indicates that the mutant has a lower fitness compared to the growth-adapted cells. For example in (**F**), a Newborn community had 70 M and 30 H. 90% of M were growth-adapted and had upper bound $g_{Mmax} = 0.7$ ("upper bound"). 10% of M had $g_{Mmax} = 0.63$, 10% less than the upper bound ("mutant"). The ratio between "mutant" and "upper bound" cells declined over maturation time, indicating that mutant M cells had a lower fitness. (**E**, **J**) When $f_P = 0.13$ (black dashed line) but not when $f_P = 0.41$ (magenta line), increasing M's affinity for Resource $(1/K_{MR})$ slightly decreases individual fitness, and barely affects community function.

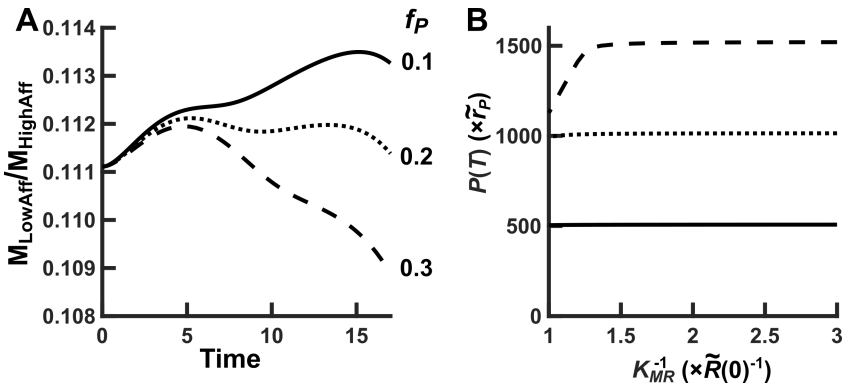

Figure S27: **At low f_P, M's lower affinity for Resource can increase its growth rate. (A)** The ratio between M_{LowAff} with low affinity for R ($K_{MR}^{-1} = 2.5\tilde{R}(0)^{-1}$) and $M_{HighAff}$ with high affinity for R ($K_{MR}^{-1} = 3\tilde{R}(0)^{-1}$) when their f_P is equal to 0.1 (solid line), 0.2 (dotted line) and 0.3 (dashed line) are plotted over one maturation cycle. **(B)** $P(T)$ improves over increasing affinity K_{MR}^{-1} when f_P is 0.1 (solid line), 0.2 (dotted line) and 0.3 (dashed line). The dependence of $P(T)$ on K_{MR}^{-1} is rather weak for low f_P. For example, when K_{MR}^{-1} increases from 1 to 3, $P(T)$ increases by only 2% and 0.6% for $f_P = 0.2$ and $f_P = 0.1$, respectively.

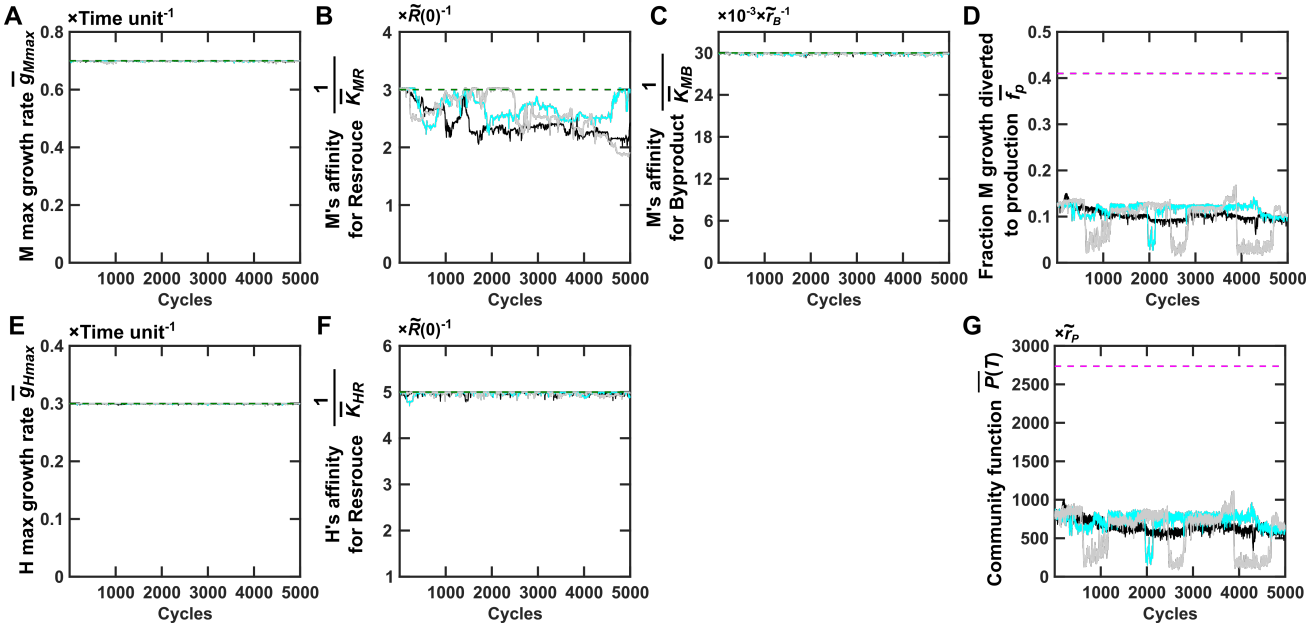

Figure S28: **Selection dynamics of communities of mono-adapted H and M when allowing all parameters to vary**. In the Newborn communities of the first cycle of community selection, all growth parameters of H and M were at their upper bounds and $f_P = f^*_{P,Mono} = 0.13$ (Figure S23). When we simulated community selection while allowing all growth parameters and f_P to vary, M's affinity for R $1/\bar{K}_{MR}$ decreased slightly because at low $f_P = 0.13$, M with a lower affinity for R (lower $1/K_{MR}$) has a slightly improved individual fitness (Figure S27). Other growth parameters ($\bar{g}_{Mmax}$, $\bar{g}_{Hmax}$, $1/\bar{K}_{MB}$ and $1/\bar{K}_{HR}$) remain mostly constant during community selection because mutants with lower-than-maximal values were selected against by natural selection and by artificial selection for higher community function (Figure S26). Other legend details can be found in Figure S9.

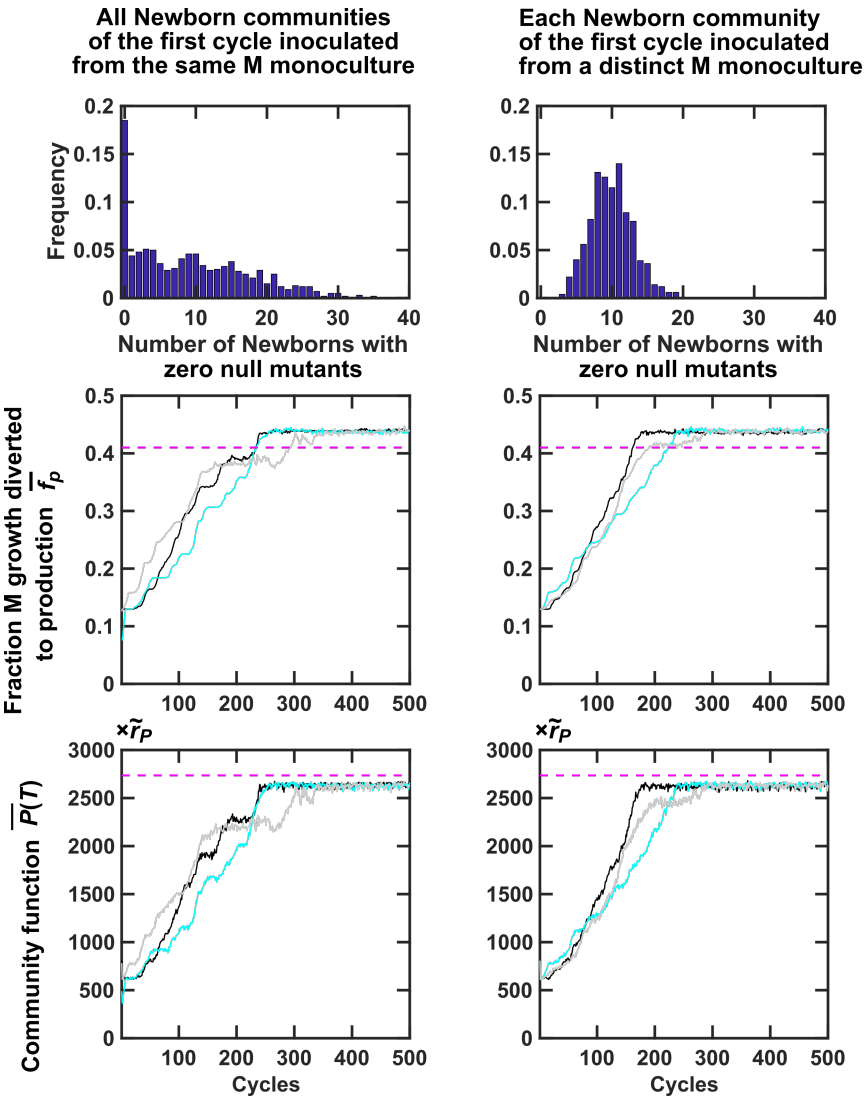

Figure S29: **Different methods of pre-growth had limited impact on selection dynamics.** (**Top Panels**) Histograms of the number of Newborn communities free of non-producer M mutants when Newborn communities from the first cycle were inoculated from a single M monoculture (**Left panel**) or from independently-grown M monocultures (**Right panel**). (**Middle and Bottom panels**) Improvement in $\overline{f}_P(T)$ and $\overline{P}(T)$ was only slightly slower when Newborn communities from the first cycle were inoculated by the same M monoculture (**Left panel**) than by distinct monocultures (**Right panel**). Here we assumed that each M monoculture grew from a single non-null M cell. This M cell went through ~23 doublings and therefore multiplied into $\sim 10^7$ cells. Every time a non-null M cell divides, the mother and daughter cells can independently mutate and become a null M cell ($f_P = 0$) at a fixed probability of 10^{-3}. If a non-null M cell has $f_P = 0.13$, then it will grow at a rate 87% of that of a null cell. After ~23 doublings, the M monocultures have on average ~3% null mutants. 60 randomly-chosen M cells from the same monoculture or from distinct monocultures, together with 40 H cells, were used to inoculate each of the 100 Newborns for the first selection cycle. To generate the histograms in (**Top panel**), the pre-growth and inoculation process was repeated 100 times.

References

[1] Trevor D. Lawley, Simon Clare, Alan W. Walker, Mark D. Stares, Thomas R. Connor, Claire Raisen, David Goulding, Roland Rad, Fernanda Schreiber, Cordelia Brandt, Laura J. Deakin, Derek J. Pickard, Sylvia H. Duncan, Harry J. Flint, Taane G. Clark, Julian Parkhill, and Gordon Dougan. Targeted restoration of the intestinal microbiota with a simple, defined bacteriotherapy resolves relapsing Clostridium difficile disease in mice. *PLoS pathogens*, 8(10):e1002995, 2012.

[2] Stefanie Widder, Rosalind J. Allen, Thomas Pfeiffer, Thomas P. Curtis, Carsten Wiuf, William T. Sloan, Otto X. Cordero, Sam P. Brown, Babak Momeni, Wenying Shou, Helen Kettle, Harry J. Flint, Andreas F. Haas, Béatrice Laroche, Jan-Ulrich Kreft, Paul B. Rainey, Shiri Freilich, Stefan Schuster, Kim Milferstedt, Jan R. van der Meer, Tobias Groβkopf, Jef Huisman, Andrew Free, Cristian Picioreanu, Christopher Quince, Isaac Klapper, Simon Labarthe, Barth F. Smets, Harris Wang, Isaac Newton Institute Fellows, and Orkun S. Soyer. Challenges in microbial ecology: building predictive understanding of community function and dynamics. *The ISME Journal*, March 2016. 00001.

[3] Stephen R. Lindemann, Hans C. Bernstein, Hyun-Seob Song, Jim K. Fredrickson, Matthew W. Fields, Wenying Shou, David R. Johnson, and Alexander S. Beliaev. Engineering microbial consortia for controllable outputs. *The ISME Journal*, 10(9):2077–2084, September 2016.

[4] Jian Zhou, Qian Ma, Hong Yi, Lili Wang, Hao Song, and Ying-Jin Yuan. Metabolome profiling reveals metabolic cooperation between Bacillus megaterium and Ketogulonicigenium vulgare during induced swarm motility. *Applied and Environmental Microbiology*, 77(19):7023–7030, October 2011. 00038.

[5] R. E. Wheatley. The consequences of volatile organic compound mediated bacterial and fungal interactions. *Antonie van Leeuwenhoek*, 81(1-4):357–364, December 2002. 00123.

[6] Kwang-sun Kim, Soohyun Lee, and Choong-Min Ryu. Interspecific bacterial sensing through airborne signals modulates locomotion and drug resistance. *Nature Communications*, 4:1809, 2013.

[7] Matthew F Traxler, Jeramie D Watrous, Theodore Alexandrov, Pieter C Dorrestein, and Roberto Kolter. Interspecies interactions stimulate diversification of the Streptomyces coelicolor secreted metabolome. *mBio*, 4(4), 2013.

[8] William Swenson, David Sloan Wilson, and Roberta Elias. Artificial ecosystem selection. *Proceedings of the National Academy of Sciences*, 97:9110–9114, 2000.

[9] W. Swenson, J. Arendt, and D.S. Wilson. Artificial selection of microbial ecosystems for 3-chloroaniline biodegradation. *Environ Microbiol*, 2(5):564–71, October 2000.

[10] Hywel T. P. Williams and Timothy M. Lenton. Artificial selection of simulated microbial ecosystems. *Proceedings of the National Academy of Sciences*, 104(21):8918–8923, May 2007. 00036.

[11] Kevin Panke-Buisse, Angela C Poole, Julia K Goodrich, Ruth E Ley, and Jenny Kao-Kniffin. Selection on soil microbiomes reveals reproducible impacts on plant function. *The ISME journal*, 9(4):980, 2015.

[12] Ulrich G Mueller, Thomas Juenger, Melissa Kardish, Alexis Carlson, Kathleen Burns, Chad Smith, and David De Marais. Artificial microbiome-selection to engineer microbiomes that confer salt-tolerance to plants. *bioRxiv*, page 081521, 2016.

[13] Charles J Goodnight. The influence of environmental variation on group and individual selection in a cress. *Evolution*, 39(3):545–558, 1985.

[14] Mitch D Day, Daniel Beck, and James A Foster. Microbial communities as experimental units. *Bioscience*, 61(5):398–406, 2011.

[15] U. G. Mueller and J. L. Sachs. Engineering Microbiomes to Improve Plant and Animal Health. *Trends in Microbiology*, 23(10):606–617, October 2015.

[16] Haoran Zhang, Brian Pereira, Zhengjun Li, and Gregory Stephanopoulos. Engineering escherichia coli coculture systems for the production of biochemical products. *Proceedings of the National Academy of Sciences*, page 201506781, 2015.

[17] James A Damore and Jeff Gore. Understanding microbial cooperation. *Journal of theoretical biology*, 299:31–41, 2012.

[18] Babak Momeni, Li Xie, and Wenying Shou. Lotka-volterra pairwise modeling fails to capture diverse pairwise microbial interactions. *Elife*, 6, 2017.

[19] Burton Simon, Jeffrey A Fletcher, and Michael Doebeli. Hamilton's rule in multi-level selection models. *Journal of theoretical biology*, 299:55–63, 2012.

[20] Jeremy J. Minty, Marc E. Singer, Scott A. Scholz, Chang-Hoon Bae, Jung-Ho Ahn, Clifton E. Foster, James C. Liao, and Xiaoxia Nina Lin. Design and characterization of synthetic fungal-bacterial consortia for direct production of isobutanol from cellulosic biomass. *Proceedings of the National Academy of Sciences*, 110(36):14592–14597, September 2013. 00024 PMID: 23959872.

[21] Kang Zhou, Kangjian Qiao, Steven Edgar, and Gregory Stephanopoulos. Distributing a metabolic pathway among a microbial consortium enhances production of natural products. *Nature biotechnology*, 2015.

[22] Hyun-Dong Shin, Shara McClendon, Trinh Vo, and Rachel R. Chen. Escherichia coli Binary Culture Engineered for Direct Fermentation of Hemicellulose to a Biofuel. *Applied and Environmental Microbiology*, 76(24):8150–8159, December 2010. 00000.

[23] T Mankad and HR Bungay. Model for microbial growth with more than one limiting nutrient. *Journal of biotechnology*, 7(2):161–166, 1988.

[24] Sattar Taheri-Araghi, Serena Bradde, John T. Sauls, Norbert S. Hill, Petra Anne Levin, Johan Paulsson, Massimo Vergassola, and Suckjoon Jun. Cell-Size Control and Homeostasis in Bacteria. *Current Biology*, 25(3):385–391, February 2015.

[25] Richard E Lenski and Michael Travisano. Dynamics of adaptation and diversification: a 10,000-generation experiment with bacterial populations. *Proceedings of the National Academy of Sciences*, 91(15):6808–6814, 1994.

[26] Adam James Waite and Wenying Shou. Adaptation to a new environment allows cooperators to purge cheaters stochastically. *Proceedings of the National Academy of Sciences*, 109(47):19079–19086, 2012.

[27] Paul B Rainey and Katrina Rainey. Evolution of cooperation and conflict in experimental bacterial populations. *Nature*, 425(6953):72, 2003.

[28] Rafael U Ibarra, Jeremy S Edwards, and Bernhard O Palsson. Escherichia coli k-12 undergoes adaptive evolution to achieve in silico predicted optimal growth. *Nature*, 420(6912):186, 2002.

[29] Rafael Sanjuán, Andrés Moya, and Santiago F Elena. The distribution of fitness effects caused by single-nucleotide substitutions in an rna virus. *Proceedings of the National Academy of Sciences of the United States of America*, 101(22):8396–8401, 2004.

[30] Karen S Sarkisyan, Dmitry A Bolotin, Margarita V Meer, Dinara R Usmanova, Alexander S Mishin, George V Sharonov, Dmitry N Ivankov, Nina G Bozhanova, Mikhail S Baranov, Onuralp Soylemez, et al. Local fitness landscape of the green fluorescent protein. *Nature*, 533(7603):397–401, 2016.

[31] Dominika M Wloch, Krzysztof Szafraniec, Rhona H Borts, and Ryszard Korona. Direct estimate of the mutation rate and the distribution of fitness effects in the yeast saccharomyces cerevisiae. *Genetics*, 159(2):441–452, 2001.

[32] Celia Payen, Anna B Sunshine, Giang T Ong, Jamie L Pogachar, Wei Zhao, and Maitreya J Dunham. High-throughput identification of adaptive mutations in experimentally evolved yeast populations. *PLoS genetics*, 12(10):e1006339, 2016.

[33] Wenying Shou, Sri Ram, and Jose M. G. Vilar. Synthetic cooperation in engineered yeast populations. *Proceedings of the National Academy of Sciences of the United States of America*, 104(6):1877–1882, February 2007. 00137.

[34] Babak Momeni, Kristen A Brileya, Matthew W Fields, and Wenying Shou. Strong inter-population cooperation leads to partner intermixing in microbial communities. *eLife*, 2, January 2013.

[35] W. D. Hamilton. The genetical evolution of social behaviour I and II. *Journal of Theoretical Biology*, 7(1):1–52, July 1964.

[36] John Maynard Smith. Group Selection and Kin Selection. *Nature*, 201(4924):1145–1147, March 1964.

[37] Sewall Wright. Tempo and Mode in Evolution: A Critical Review. *Ecology*, 26(4):415–419, 1945.

[38] George R. Price. Selection and Covariance. *Nature*, 227(5257):520–521, August 1970. 01240.

[39] Michael J. Wade. A Critical Review of the Models of Group Selection. *The Quarterly Review of Biology*, 53(2):101–114, June 1978. ArticleType: research-article / Full publication date: Jun., 1978 / Copyright © 1978 The University of Chicago Press.

[40] William M Muir. Group selection for adaptation to multiple-hen cages: selection program and direct responses. *Poultry Science*, 75(4):447–458, 1996.

[41] David C. Queller and Joan E. Strassmann. Kin Selection and Social Insects. *BioScience*, 48(3):165–175, March 1998.

[42] Michael J Wade. An experimental study of kin selection. *Evolution*, pages 844–855, 1980.

[43] Arne Traulsen and Martin A. Nowak. Evolution of cooperation by multilevel selection. *Proceedings of the National Academy of Sciences*, 103(29):10952–10955, July 2006.

[44] L. Lehmann, L. Keller, S. West, and D. Roze. Group selection and kin selection: Two concepts but one process. *Proc Natl Acad Sci USA*, 104(16):6736–6739, April 2007.

[45] Benjamin Kerr. Theoretical and experimental approaches to the evolution of altruism and the levels of selection. *Experimental Evolution: Concepts, Methods, and Applications of Selection Experiments*, pages 585–630, 2009. 00006.

[46] Herwig Bachmann, Frank J Bruggeman, Douwe Molenaar, Filipe Branco dos Santos, and Bas Teusink. Public goods and metabolic strategies. *Current Opinion in Microbiology*, 31:109–115, June 2016. 00000.

[47] Katrin Hammerschmidt, Caroline J. Rose, Benjamin Kerr, and Paul B. Rainey. Life cycles, fitness decoupling and the evolution of multicellularity. *Nature*, 515(7525):75–79, November 2014.

[48] Martin A. Nowak. Five Rules for the Evolution of Cooperation. *Science*, 314(5805):1560–1563, December 2006.

[49] C. J. Goodnight and L. Stevens. Experimental studies of group selection: what do they tell us about group selection in nature? *The American Naturalist*, 150 Suppl 1:S59–79, July 1997.

[50] Samuel Frederick Mock Hart, David Skelding, Adam J Waite, Justin Burton, Li Xie, and Wenying Shou. Microscopy quantification of microbial birth and death dynamics. *bioRxiv*, page 324269, 2018.

[51] Kristina L Hillesland and David A Stahl. Rapid evolution of stability and productivity at the origin of a microbial mutualism. *Proceedings of the National Academy of Sciences*, 107(5):2124–2129, 2010.

[52] D. S. Wilson. A theory of group selection. *Proceedings of the National Academy of Sciences*, 72(1):143–146, January 1975.

[53] Michael E Gilpin. *Group selection in predator-prey communities*, volume 9. Princeton University Press, 1975.

[54] J. Maynard Smith. Group Selection. *The Quarterly Review of Biology*, 51(2):277–283, June 1976.

[55] Michael Doebeli, Yaroslav Ispolatov, and Burt Simon. Towards a mechanistic foundation of evolutionary theory. *eLife*, 6:e23804, February 2017.

[56] L. Chao and B.R. Levin. Structured habitats and the evolution of anticompetitor toxins in bacteria. *Proc Natl Acad Sci U S A*, 78(10):6324–8, October 1981.

[57] Herwig Bachmann, Martin Fischlechner, Iraes Rabbers, Nakul Barfa, Filipe Branco dos Santos, Douwe Molenaar, and Bas Teusink. Availability of public goods shapes the evolution of competing metabolic strategies. *Proceedings of the National Academy of Sciences of the United States of America*, 110(35):14302–14307, August 2013.

[58] John S Chuang, Olivier Rivoire, and Stanislas Leibler. Simpson's paradox in a synthetic microbial system. *Science (New York, N.Y.)*, 323(5911):272–275, January 2009.

[59] George R Price. Extension of covariance selection mathematics. *Annals of human genetics*, 35(4):485–490, 1972.

[60] Li Xie and Wenying Shou. Community function landscape and steady state species composition shape the eco-evolutionary dynamics of arti1cial community selection. *bioRxiv*, page 264697, 2018.

[61] Samuel FM Hart, Hanbing Mi, Robin Green, Li Xie, Jose Mario Bello Pineda, Babak Momeni, and Wenying Shou. Resolving challenges in quantitative modeling of microbial community dynamics. *bioRxiv*, page 356519, 2018.

[62] John L Spudich and Daniel E Koshland Jr. Non-genetic individuality: chance in the single cell. *Nature*, 262(5568):467, 1976.

[63] Stephen T Chisholm, Gitta Coaker, Brad Day, and Brian J Staskawicz. Host-microbe interactions: shaping the evolution of the plant immune response. *Cell*, 124(4):803–814, 2006.

[64] Ruth E Ley, Micah Hamady, Catherine Lozupone, Peter J Turnbaugh, Rob Roy Ramey, J Stephen Bircher, Michael L Schlegel, Tammy A Tucker, Mark D Schrenzel, Rob Knight, et al. Evolution of mammals and their gut microbes. *Science*, 320(5883):1647–1651, 2008.

[65] Kevin R Foster, Jonas Schluter, Katharine Z Coyte, and Seth Rakoff-Nahoum. The evolution of the host microbiome as an ecosystem on a leash. *Nature*, 548(7665):43, 2017.

[66] Luc De Vuyst, Raf Callewaert, and Kurt Crabbé. Primary metabolite kinetics of bacteriocin biosynthesis by Lactobacillus amylovorus and evidence for stimulation of bacteriocin production under unfavourable growth conditions. *Microbiology*, 142(4):817–827, 1996.

[67] Melanie JI Müller, Beverly I Neugeboren, David R Nelson, and Andrew W Murray. Genetic drift opposes mutualism during spatial population expansion. *Proceedings of the National Academy of Sciences*, 111(3):1037–1042, 2014.

[68] Thomas Egli. *Nutrition, microbial*. Oxford: Elsevier Academic Press, 2009.

[69] Kai Zhuang, Goutham N Vemuri, and Radhakrishnan Mahadevan. Economics of membrane occupancy and respiro-fermentation. *Molecular systems biology*, 7(1):500, 2011.

[70] Joan B Peris, Paulina Davis, José M Cuevas, Miguel R Nebot, and Rafael Sanjuán. Distribution of fitness effects caused by single-nucleotide substitutions in bacteriophage f1. *Genetics*, 185(2):603–609, 2010.

[71] Adrian WR Serohijos and Eugene I Shakhnovich. Merging molecular mechanism and evolution: theory and computation at the interface of biophysics and evolutionary population genetics. *Current opinion in structural biology*, 26:84–91, 2014.

[72] Adam Eyre-Walker and Peter D Keightley. The distribution of fitness effects of new mutations. *Nature reviews. Genetics*, 8(8):610, 2007.

[73] Michael A Stiffler, Doeke R Hekstra, and Rama Ranganathan. Evolvability as a function of purifying selection in tem-1 β-lactamase. *Cell*, 160(5):882–892, 2015.

[74] John W Drake. A constant rate of spontaneous mutation in dna-based microbes. *Proceedings of the National Academy of Sciences*, 88(16):7160–7164, 1991.

[75] Gregory I. Lang and Andrew W. Murray. Estimating the Per-Base-Pair Mutation Rate in the Yeast Saccharomyces cerevisiae. *Genetics*, 178(1):67–82, January 2008.

[76] Sasha F Levy, Jamie R Blundell, Sandeep Venkataram, Dmitri A Petrov, Daniel S Fisher, and Gavin Sherlock. Quantitative evolutionary dynamics using high-resolution lineage tracking. *Nature*, 519(7542):181, 2015.

[77] Clifford Zeyl and J Arjan GM DeVisser. Estimates of the rate and distribution of fitness effects of spontaneous mutation in saccharomyces cerevisiae. *Genetics*, 157(1):53–61, 2001.

[78] Jeffrey E Barrick, Dong Su Yu, Sung Ho Yoon, Haeyoung Jeong, Tae Kwang Oh, Dominique Schneider, Richard E Lenski, and Jihyun F Kim. Genome evolution and adaptation in a long-term experiment with escherichia coli. *Nature*, 461(7268):1243, 2009.

[79] Toon Swings, Bram Van den Bergh, Sander Wuyts, Eline Oeyen, Karin Voordeckers, Kevin J Verstrepen, Maarten Fauvart, Natalie Verstraeten, and Jan Michiels. Adaptive tuning of mutation rates allows fast response to lethal stress in escherichia coli. *eLife*, 6(22939), 2017.

[80] Lília Perfeito, Lisete Fernandes, Catarina Mota, and Isabel Gordo. Adaptive mutations in bacteria: high rate and small effects. *Science*, 317(5839):813–815, 2007.

[81] John H Gillespie. Molecular evolution over the mutational landscape. *Evolution*, 38(5):1116–1129, 1984.

[82] H Allen Orr. The distribution of fitness effects among beneficial mutations. *Genetics*, 163(4):1519–1526, 2003.

[83] Marianne Imhof and Christian Schlötterer. Fitness effects of advantageous mutations in evolving escherichia coli populations. *Proceedings of the National Academy of Sciences*, 98(3):1113–1117, 2001.

[84] Rees Kassen and Thomas Bataillon. Distribution of fitness effects among beneficial mutations before selection in experimental populations of bacteria. *Nature genetics*, 38(4):484, 2006.

[85] Darin R Rokyta, Paul Joyce, S Brian Caudle, and Holly A Wichman. An empirical test of the mutational landscape model of adaptation using a single-stranded dna virus. *Nature genetics*, 37(4):441, 2005.

[86] Darin R Rokyta, Craig J Beisel, Paul Joyce, Martin T Ferris, Christina L Burch, and Holly A Wichman. Beneficial fitness effects are not exponential for two viruses. *Journal of molecular evolution*, 67(4):368, 2008.

[87] Michael J Wiser, Noah Ribeck, and Richard E Lenski. Long-term dynamics of adaptation in asexual populations. *Science*, 342(6164):1364–1367, 2013.

[88] Lukasz Jasnos and Ryszard Korona. Epistatic buffering of fitness loss in yeast double deletion strains. *Nature genetics*, 39(4):550, 2007.

[89] Rafael Sanjuán, Andrés Moya, and Santiago F Elena. The contribution of epistasis to the architecture of fitness in an rna virus. *Proceedings of the National Academy of Sciences of the United States of America*, 101(43):15376–15379, 2004.

[90] Aisha I Khan, Duy M Dinh, Dominique Schneider, Richard E Lenski, and Tim F Cooper. Negative epistasis between beneficial mutations in an evolving bacterial population. *Science*, 332(6034):1193–1196, 2011.

[91] Santiago F Elena and Richard E Lenski. Test of synergistic interactions among deleterious mutations in bacteria. *Nature*, 390(6658):395, 1997.

[92] Carlos L Araya, Douglas M Fowler, Wentao Chen, Ike Muniez, Jeffery W Kelly, and Stanley Fields. A fundamental protein property, thermodynamic stability, revealed solely from large-scale measurements of protein function. *Proceedings of the National Academy of Sciences*, 109(42):16858–16863, 2012.

[93] Hsin-Hung Chou, Hsuan-Chao Chiu, Nigel F Delaney, Daniel Segrè, and Christopher J Marx. Diminishing returns epistasis among beneficial mutations decelerates adaptation. *Science*, 332(6034):1190–1192, 2011.

[94] Sergey Kryazhimskiy, Daniel P Rice, Elizabeth R Jerison, and Michael M Desai. Global epistasis makes adaptation predictable despite sequence-level stochasticity. *Science*, 344(6191):1519–1522, 2014.

[95] G. W. Luli and W. R. Strohl. Comparison of growth, acetate production, and acetate inhibition of Escherichia coli strains in batch and fed-batch fermentations. *Applied and Environmental Microbiology*, 56(4):1004–1011, April 1990.

[96] Wenying Shou. Acknowledging selection at sub-organismal levels resolves controversy on pro-cooperation mechanisms. *eLife*, page e10106, December 2015.

[97] R C Lewontin. The Units of Selection. *Annual Review of Ecology and Systematics*, 1(1):1–18, 1970.

[98] A. Crameri, E. A. Whitehorn, E. Tate, and W. P. Stemmer. Improved green fluorescent protein by molecular evolution using DNA shuffling. *Nature Biotechnology*, 14(3):315–319, March 1996.

[99] Manfred T. Reetz and José Daniel Carballeira. Iterative saturation mutagenesis (ISM) for rapid directed evolution of functional enzymes. *Nature Protocols*, 2(4):891–903, April 2007.

[100] Eric T. Boder, Katarina S. Midelfort, and K. Dane Wittrup. Directed evolution of antibody fragments with monovalent femtomolar antigen-binding affinity. *Proceedings of the National Academy of Sciences*, 97(20):10701–10705, September 2000.